Cellular and molecular basis of leptin resistance

Authors

Bowen Tan[1,*], Kristina Hedbacker[1,*], Leah Kelly[1], Zhaoyue Zhang[1], Ji-Dung Luo[2], Joshua D. Rabinowitz[3,4,5], Jeffrey M. Friedman[1,§]

[1] Laboratory of Molecular Genetics, Howard Hughes Medical Institute, The Rockefeller University, New York, NY 10065, USA.
[2] Bioinformatics Resource Center, The Rockefeller University, New York, NY 10065, USA
[3] Department of Chemistry, Princeton University, Princeton, NJ, USA.
[4] Lewis-Sigler Institute of Integrative Genomics, Princeton University, Princeton, NJ, USA.
[5] Ludwig Institute for Cancer Research, Princeton University, Princeton, NJ, USA.
[*] These authors contribute equally.

[§] Correspondence should be addressed to: Jeffrey M. Friedman, friedj@rockefeller.edu

Abstract:

Diet-induced obese (DIO) mice and obese humans have high circulating levels of leptin and do not respond to the exogenous hormone suggesting that they develop leptin resistance. However, the underlying cellular and molecular mechanisms that reduce leptin signaling are unknown. As part of a metabolomic screen for biomarkers of a leptin effect, we found that leptin reduced the level of leucine and methionine, mTOR ligands, only in leptin-sensitive animals, raising the possibility that mTOR activation might contribute to leptin resistance. We tested this by first treating DIO, chow-fed, *ob/ob* and *db/db* mice with rapamycin, an mTOR inhibitor. Rapamycin reduced food intake and adiposity in DIO mice but not in *ob/ob* or *db/db* animals. Whole-brain mapping revealed that the levels of phosphoS6, a marker of mTOR activity, were increased in the arcuate nucleus (ARC) and other hypothalamic nuclei in DIO mice. Subsequent multi-modal single-nucleus RNA sequencing of the ARC in DIO, chow-fed and *ob/ob* mice revealed that rapamycin altered gene expression exclusively in POMC neurons of DIO mice which also showed normalization of pSTAT3 levels after rapamycin treatment. Consistent with an effect on POMC neurons, rapamycin did not alter food intake or adiposity in mice after an ablation of POMC neurons or in MC4R knockout mice. In contrast, a POMC-specific deletion of *Tsc1*, which leads to a cell specific increase of mTOR activity, resulted in leptin resistance in chow-fed animals and reduced leptin sensitivity in these and *ob/ob* mice. In *ob/ob*-POMC$^{tsc1\text{-}/\text{-}}$ mice, rapamycin did not reduce food intake or adiposity in the absence of leptin. Finally, POMC-specific deletion of mTOR activators decreased the weight gain in mice fed a HFD. These data suggest that leptin resistance in DIO mice is the result of increased mTOR activity in POMC neurons and that inhibition of mTOR reduces obesity by reversing leptin resistance.

Introduction

Obesity is the cardinal feature of the metabolic syndrome and a worldwide public health problem [1]. Obesity develops when food intake exceeds energy expenditure leading to deposition of excess adipose tissue. In lean animals, adipose tissue mass is tightly controlled by the hormone leptin which functions as the afferent signal in a negative feedback loop regulating energy balance. Leptin acts on key neural populations in hypothalamus to control food intake and mutations that alter signaling by leptin or melanocortin, downstream mediators of leptin action, cause extreme obesity in humans and rodents. Leptin reduces appetite by activating αMSH (POMC) expressing neurons in the arcuate nucleus of the hypothalamus and most of the known mutations that cause obesity alter the production of αMSH or its target, the MC4R G protein coupled receptor. Animals with leptin receptor or melanocortin mutations become hyperleptinemic and show a reduced response to exogenous leptin which are the hallmarks of a hormone resistance syndrome [2,3]. These leptin resistant animals also show a reduced biochemical response to the exogenous hormone in POMC neurons with abrogated phosphorylation of the STAT3 transcription factor [4-6].

Leptin resistance can also be acquired when mice are fed a high fat diet (HFD) leading to Diet Induced Obesity (DIO) but, in contrast to animals with mutations in the leptin-melanocortin axis, the pathogenesis of diet-induced leptin resistance has not been determined. Similar to DIO mice, most obese humans also develop leptin resistance and the response of DIO mice to anti-obesity therapies is highly predictive of a human response [7,8]. Thus delineating the pathogenesis of leptin resistance in DIO mice would advance our understanding of the pathogenesis of obesity. In contrast, the pathogenesis of insulin resistance is still poorly understood, and these findings might also have general implications by illuminating a cause of an acquired hormone resistance syndrome. Reversing leptin resistance could also have clinical implications particularly since leptin spares lean body mass in contrast to the new peptide-based therapeutics that can cause significant loss of lean mass [9].

Here we present a comprehensive set of physiologic, genetic and neurobiological studies showing that increased activity of the mTOR kinase in POMC neurons is necessary and sufficient for the development of leptin resistance and obesity in DIO mice.

Results

A Metabolomic Screen for Biomarkers for Leptin Resistance

Animals and humans with low leptin levels lose weight on leptin therapy and we initially sought to identify acute biomarkers of a leptin response as a possible means for identifying responders even before weight loss develops [3,7,8]. Toward that end, we collected plasma from leptin-sensitive and leptin-resistant animals before and after leptin treatment, controlling for food intake and dietary composition among four groups: wild-type mice fed chow (WT-Chow) or a high-fat diet (WT-DIO), and *ob/ob* mice fed chow (OB-Chow) or a high-fat diet (OB-HFD). The OB-Chow group was pair-fed to the WT-Chow group and the OB-HFD group was pair-fed to the WT-DIO group, all for 18 weeks (Fig. 1a). Growth curves revealed that the WT-Chow group remained lean while the other three groups became increasingly obese (Fig. 1b, c, S1e, f). Plasma was collected from all the animals after vehicle treatment at week 18, and again after leptin treatment at week 19 (Fig. 1a). As expected, acute leptin treatment decreased food intake and body weight in the WT-Chow, OB-Chow and OB-HFD groups but did not affect the leptin-resistant WT-DIO group (Fig. 1d). Plasma metabolites were measured and analyzed using hierarchical clustering based on levels of metabolites in the four groups after leptin treatment (Fig. 1e, S1a, b). In these analyses we sought pairwise, same-trend alterations in leptin-sensitive and resistant WT-DIO mice in response to vehicle vs. leptin. As previously reported [10], leptin decreased plasma triglycerides in leptin-sensitive mice but not in WT-DIO mice (Fig. 1f). We also found an increased level of several phosphatidic acids and glucosyl ceramides after leptin treatment of WT-DIO mice but not in the other three groups (Fig. 1h, i), raising the possibility that leptin prevented the accumulation of these metabolites in the sensitive animals. Finally, we found a significant decrease of plasma leucine and methionine levels in leptin-sensitive but not in WT-DIO mice (Fig. 1g, S1c). Leucine and methionine are canonical activators of the mTOR pathway, and phosphatidic acids and ceramides can also modulate the PI3K-mTOR pathway [11-13]. Our finding that leptin sensitivity was inversely associated with plasma levels of these mTOR ligands led us to hypothesize that mTOR activation might diminish leptin sensitivity in DIO mice. We evaluated this possibility by treating DIO and mutant obese mice with rapamycin, a specific mTOR inhibitor.

Rapamycin Reduces Obesity by Re-sensitizing Endogenous Leptin Signaling

DIO mice were treated with daily intraperitoneal (i.p.) injections of rapamycin (RAP) or vehicle (VEH) for 10 weeks. The rapamycin-treated DIO mice showed a decrease in daily and cumulative food intake (RAP 149.1 ± 4.1 g vs. VEH 186.6 ± 5.5 g; $p<0.001$), body weight (RAP -27.6 ± 2.0 % vs. VEH 3.7 ± 2.1 %; $p<0.0001$), fat mass (RAP 34.1 ± 3.0 % vs. VEH 49.6 ± 1.3 %; $p<0.0001$), and a small decrease in lean mass (RAP 26.1 ± 0.6 g vs. VEH 28.9 ± 0.4 g; $p<0.001$) (Fig. 2a-d, S2j). Thus, similar to the reported effects of leptin on leptin-sensitive animals[2], rapamycin reduced food intake, body weight and preferentially reduced fat mass relative to lean mass in DIO animals (Fig. 2c, d). Similar to the effect of 10 weeks of rapamycin treatment, 14-day rapamycin treatment of DIO mice also decreased food intake (RAP 32.4 ± 1.6 g vs. VEH 39.7 ± 1.9 g; $p<0.001$), body weight (RAP -10.2 ± 1.1 % vs. VEH 0.1 ± 1.1 %; $p<0.0001$) and fat mass (RAP 41.5 ± 1.8 % vs. VEH 46.4 ± 1.4 %; $p<0.05$). In this 14-day experiment, lean mass was unchanged after rapamycin treatment (Fig. 2e-h, S2i). In contrast, rapamycin had little or no effect on food intake, body weight or fat mass in chow fed lean mice. These animals are leptin sensitive with low endogenous hormone levels. (Fig. 2i-l, S2k). The failure of rapamycin to reduce weight in lean animals with low endogenous leptin levels led us to hypothesize that it synergizes with leptin. Consistent with the possibility, a combination of low-dose leptin (150 ng/hr) plus rapamycin led to even greater weight loss, reduction of food intake and diminished fat mass in lean chow fed mice compared to chow fed animals treated with high-dose leptin (600 ng/hour) alone (low-dose LEP+RAP vs. high-dose LEP; Weight: -10.1 ± 1.0 %

vs. -8.6 ± 2.4 %; p = ns, Food intake: 59.8 ± 5.9 g vs. 53.9 ± 3.4 g; p=ns, Fat mass: -3.7 ± 1.0 % vs. -3.6 ± 0.9 %; p = ns) (Fig. S3a-h). There was no change in lean mass in any of these groups (Fig. S3d, h). Finally, treatment of lean chow-fed mice with rapamycin together with a high physiologic dose of leptin (600 ng/hr) showed a further reduction of food intake and body weight than did animals treated with either agent alone (Fig. 2i-l). These data suggested that rapamycin might potentiate leptin signaling to reduce food intake and adiposity. If rapamycin-mediated weight loss in DIO mice is dependent on their elevated endogenous leptin levels, rapamycin should have minimal effects in *ob/ob* and *db/db* mice that carry mutations in leptin and the leptin receptor. Consistent with this, rapamycin did not decrease food intake or fat mass in *ob/ob* and *db/db* mice (Fig. 2m-t, S2l, m). Leptin-mediated weight loss in sensitive mice is primarily confined to fat mass and rapamycin did cause a small decrease of lean mass which has previously been reported (Fig. 2n-p, r-t) [14]. To control for dietary effects, *ob/ob* and *db/db* mice were also fed a HFD and then treated with rapamycin. Here again, there was no effect on food intake or fat mass (Fig. S2a-h, n, o). Aged mice also become leptin resistant and obese [15] and we thus tested the effects of rapamycin on leptin sensitivity in 16-month-old animals. Though not as obese as DIO mice, these 16-month-old mice were overweight at baseline (35.9 ± 0.9 g; n = 13), and leptin treatment alone only mildly altered food intake and body weight. However the combination of rapamycin with leptin treatment of aged mice significantly reduced food intake (LEP+RAP 46.9 ± 3.8 g vs. LEP 57.3 ± 4.8 g; p<0.05) body weight (LEP+RAP -13.8 ± 3.3 % vs. LEP -5.4 ± 2.8 %; p<0.01) and fat mass (LEP+RAP -12.2 ± 6.1 % vs. LEP -7.6 ± 3.8 %; p<0.05) with no significant effect on lean mass (p = 0.9) (Fig. S3i-m). A table summarizing these findings is provided (Fig. S3n, o). In aggregate, these data suggest that rapamycin sensitizes DIO and aged obese mice to their endogenous leptin. We next evaluated if pre-treatment of DIO mice with rapamycin restored the response to exogenous leptin.

DIO mice were pre-treated with rapamycin or vehicle for three weeks, after which they were treated with either leptin or vehicle for three days (Fig. 3a). Leptin elicited a further decrease in food intake (9.6 ± 0.9 g vs. 7.2 ± 0.9 g; p<0.01) (Fig. 3c) and body weight (1.6 ± 0.5 % vs. -2.9 ± 0.9 %; p<0.01) (Fig. 3d) in DIO mice pre-treated with rapamycin compared to those pre-treated with vehicle. Because pre-treatment with rapamycin reduced the weight of DIO mice, and hence leptin levels (Fig. 3b), a separate group of DIO mice treated with vehicle was pair-fed to the rapamycin-treated group fed ad libitum on a HFD for five weeks (Fig. 3e). We then tested leptin sensitivity in the pair-fed animals. The response to leptin in these pair-fed DIO mice was significantly reduced compared to the rapamycin treated group with higher food intake (7.1 ± 0.6 g vs. 5.1 ± 0.4 g; p<0.05) and weight (+2.4 ± 1.3 % vs. -2.1 ± 0.5 %; p<0.01) (Fig. 3g, h, Fig. S4a, b). Consistent with their lower weight, the plasma leptin levels were lower in rapamycin-treated DIO mice compared to the pair-fed vehicle group (19.1 ± 3.7 ng/ml vs. 41.5 ± ng/ml; p<0.01) (Fig. 3f). We also evaluated metabolism of the DIO animals using indirect calorimetry-enabled metabolic cages and found that rapamycin-treated DIO mice exhibited a decrease of respiratory exchange ratio (RER) (RAP 0.76 ± 0.00 vs. VEH 0.78 ± 0.01; p<0.01), and an increase in energy expenditure (RAP 1.2 ± 0.1 vs. VEH 1.0 ± 0.0; p<0.05) compared to the vehicle group (Fig. S4c-f).

Rapamycin has been shown to impair glucose tolerance while leptin has been shown to improve it [16,17]. Consistent with previous studies, chronic rapamycin treatment alone increased plasma glucose levels in chow-fed lean mice, *ob/ob* and *db/db* mice (Fig. 3i, k, l) while concomitant leptin and rapamycin treatment lowered the baseline plasma glucose levels in WT-Chow, WT-DIO and OB-Chow animals (Fig. 3i, j, k). To further address an effect of leptin in mitigating the glucose intolerance seen after rapamycin treatment, we performed glucose-tolerance tests in DIO and chow fed mice. In both cases, rapamycin alone worsened glucose tolerance, and the addition of exogenous leptin significantly improved the glucose intolerance induced by rapamycin. This improvement was characterized by a lower peak glucose level, a reduction of the area under the curve (WT-Chow: RAP $5.4 \times 10^4 \pm 0.3 \times 10^4$ a.u. vs. RAP+LEP

$3.2 \times 10^4 \pm 0.2 \times 10^4$ a.u.; $p<0.0001$. DIO: RAP $9.3 \times 10^4 \pm 0.9 \times 10^4$ a.u. vs. RAP+LEP $6.9 \times 10^4 \pm 0.5 \times 10^4$ a.u.; $p<0.05$) and the normalization of plasma glucose after 90-120 minutes (Fig. 3m-p). Thus, while chronic rapamycin treatment alone can impair glucose tolerance, exogenous leptin mitigates it. We next set out to study the mechanism responsible for re-sensitization of leptin signaling in DIO mice after rapamycin treatment.

The Cellular Target of Rapamycin-Mediated Leptin Re-sensitization

We identified anatomic sites with increased mTOR activity in DIO mice by performing whole-brain imaging to map levels of phosphoS6 (pS6), an mTOR substrate and canonical marker for its activity, using the SHIELD brain clearing procedure [18]. The hypothalamus showed the largest increase of pS6 levels in DIO mice compared to chow-fed mice (Fig. S5a, b). Numerous studies have shown that leptin regulates energy balance by modulating the activity of specific cell types in the hypothalamus, particularly the arcuate nucleus (ARC) [6,19,20]. We thus assayed pS6 levels in the ARC of DIO mice before and after rapamycin treatment by IHC and consistent with the SHIELD data, there were significantly elevated pS6 levels in the ARC of DIO mice compared to chow-fed lean mice that were then reduced by rapamycin treatment (Fig. 4a, k, S5a, b). We then set out to identify the specific cells showing increased pS6 levels.

We performed single-nucleus RNA sequencing (snRNA-seq) of the ARC to molecularly profile the response of individual cells to 3 days of rapamycin treatment vs. vehicle in chow-fed lean, DIO and *ob/ob* mice (Fig. 4c, S5c). This short-term treatment did not significantly alter food intake or body weight (see Fig. 2). The ARC was microdissected and single-nuclei libraries were prepared and sequenced. We used UMAP to define 18 distinct cellular clusters shared among all of the groups (Fig. 4d) and generated a violin plot of enriched molecular markers for each of them (Fig. 4e). These analyses revealed that rapamycin treatment of DIO mice significantly altered gene expressions in only a single cluster: cluster 12, which was defined by two marker genes *Pomc* and *Spag16* (Fig. 4f). There were only minimal, non-significant changes in the expression of the genes in this cluster in rapamycin-treated chow fed mice and a set of opposite changes was observed in *ob/ob* mice (Fig S5c-e). POMC neurons are a canonical target of leptin action and these data thus suggested that the subtype of POMC neurons in this cluster might be the cellular target of rapamycin in DIO mice. To further characterize the POMC clusters and other known populations, we analyzed gene expression in ARC neurons expressing canonical marker genes for other cell types controlling feeding behavior and metabolism including *Pomc+, Oxt+, Npy+, Lepr+, Insr+, Glp1r+, Ghrh+, Crh+, Cck+, Cartpt+, Bdnf+* and *Agrp+* neurons. Consistent with the analysis of genes expressed in cluster 12, *Pomc+* neurons from DIO mice showed the largest transcriptomic alterations in response to rapamycin. Prior reports have indicated there are at least two distinct subsets of POMC neurons expressing either *Lepr* or *Glp1r* [21-25]. To further evaluate which population showed significant changes after rapamycin treatment, we sub-clustered the POMC neurons into two distinct populations: POMC subtype 2 included *Lepr*, *Stat3* and *Spag16,* while POMC subtype 1 included *Htr2c*, in addition to other molecular markers differentially expressed between the two subtypes (Fig. 4h). While these two POMC subtypes were evident in the three groups, only POMC subtype 2 showed significant transcriptional changes after rapamycin treatment of DIO mice, while POMC subtype 1 did not (Fig. 4h-j). Further analysis of differentially expressed genes in POMC subtype 2 neurons from DIO mice revealed that rapamycin decreased the expression of *Ptprm* and *Ptprt*, which encode enzymes that dephosphorylate pSTAT3 [26], a key component of the leptin signal transduction pathway and *Gabrg3*, a GABA receptor subunit previously shown to inhibit POMC neurons [27,28]. Rapamycin also increased the expression of *Pomc*, the precursor of α-MSH, *Pcsk2*, a POMC processing enzyme, and *Trpm3*, a cation channel (Fig. 4j). The expression levels of these genes in POMC cluster subtype 2 were unchanged in neurons from rapamycin-treated chow fed lean mice (Fig. 4j) and rapamycin treatment of *ob/ob* mice suppressed the expression of *Pomc* and *Pcsk2* in *Pomc+* cell types (Fig. S5d, e). These findings suggest that

rapamycin restored leptin action by reducing the expression of genes that diminish leptin-melanocortin signal transduction and increasing the expression of genes that increase the levels of α-MSH, a key neuropeptide produced by POMC neurons, and possibly ion channels that could increase their neuronal activity. To assess this, we examined the effect of rapamycin on the levels of pSTAT3 and pS6 in POMC neurons in a POMC-eGFP transgenic mouse line [6]. At baseline, pS6 levels were increased in POMC neurons of DIO mice and pSTAT3 was expressed at very low levels. Three-day rapamycin treatment decreased pS6 levels in POMC neurons and significantly increased the pSTAT3 levels compared to the vehicle group. These data suggest that rapamycin reduced the weight of DIO mice by re-sensitizing POMC neurons to the high endogenous leptin levels in these animals.

We further evaluated this by analyzing the effect of rapamycin on the activity of POMC neurons with and without leptin in slices from POMC-eGFP transgenic mice. Representative cell-attached traces from POMC neurons from DIO mice pretreated with either vehicle or rapamycin for three days (Fig. 5a). Average firing rates were as follows: untreated DIO mice, 0.91 Hz ± 0.11 (n=154; p=0.007), DIO mice treated with vehicle 0.81± 0.20 (n = 36; p = 0.003, both Mann Whitney test), chow-fed mice 2.00 Hz ± 0.42 (n = 51), DIO mice pretreated with rapamycin, 2.75 ± 0.64Hz (n = 28) (Fig. 5b). Pre-treatment with rapamycin led to an increase in the baseline firing rate of POMC neurons compared to vehicle-treated DIO mice, (p = 0.0004, Fig. 5b) or untreated DIO mice (p<0.0001, both Mann Whitney test, Fig. 5b). There was also a smaller proportion of spontaneously spiking POMC neurons from DIO mice compared to the chow-fed mice (57.80%, n = 154 vs 90.2%, n = 51, p<0.0001, two tailed binomial test, Fig 5c), as has previously been reported [29]. Rapamycin pretreatment in DIO mice also led to an increase in the number of spiking neurons compared to untreated DIO mice (82.14%, n = 28; p = 0.012), or vehicle-treated DIO mice (47.22%, n = 36; p<0.0001, both binomial test, Fig 5c).

We next evaluated the response of POMC neurons to leptin with or without pretreatment with rapamycin. Leptin led to a large increase in overall firing rate of POMC neurons from chow fed mice (2.95 ± 0.34 to 4.41 ± 1.31, n = 20; p = 0.028, Fig. 5c), with a significantly smaller increase in firing rate of POMC neurons from DIO mice (1.50 ± 0.29 to 1.77 ± 0.33, n=50; p=0.0238). Rapamycin pretreatment in DIO mice resulted in a larger increase of POMC neuron firing rates in response to leptin (3.58 ± 0.88 to 4.81 ± 1.03, n=17, p=0.0208, Fig. 5c), while the firing rates from vehicle-treated DIO mice did not change significantly (1.38 ± 0.31 vs 1.87 ± 0.67, n = 18; p = 0.6095, all Wilcoxon matched pairs, Fig. 5c). Rapamycin pretreatment also increased the proportion of leptin-excited neurons to 76.5% compared to 50% (n = 18) of POMC neurons from vehicle-treated mice (n = 17; p = 0.0148, binomial test, Fig.5e).

Melanocortin Signaling is Required for Rapamycin-Mediated Leptin Sensitization.

Mice with POMC ablation have been previously shown to become obese [30], and if POMC neurons are the primary target of rapamycin, similar to *ob/ob* and *db/db* mice, these obese animals should not show a reduced fat mass after rapamycin treatment. We generated four groups of mice by stereotaxically delivering AAV5-hsyn-FLEX-mCherry or AAV5-hsyn-FLEX-dTA into the ARC of POMC-Cre mice (referred to as POMC-dTA vs. POMC-mCherry mice). Eight weeks post viral expression, the POMC-dTA mice were obese (45.5 ± 2.0 g vs. 29.0 ± 1.5 g) (Fig. S6a) with higher fat mass (42.0 ± 1.7 % vs. 14.9 ± 2.3 %; p<0.001) than the POMC-mCherry group which remained lean (Fig. 6d). Treatment of POMC-dTA animals with a high dose of leptin (600 ng/hr) had no effect on food intake, body weight or glucose tolerance confirming that these animals were leptin resistant (Fig. S6d-f). We then administered rapamycin vs. vehicle to POMC-dTA and POMC-mCherry mice (Fig. 6a) for 14 days. Rapamycin treatment of POMC-dTA mice did not significantly alter food intake (Fig. 6b. RAP 66.5 ± 4.2 g vs. VEH 78.2 ± 3.3 g; p=0.27) or fat mass (Fig. 6d. 41.5 ± 1.7 % vs. 41.8 ± 1.2 %; p=1.0). Similar to the effects in *ob/ob* and *db/db* mice there was a small decrease in weight (RAP in dTA: -7.3 ± 1.1 % vs. VEH in dTA:3.1 ± 2.1, p<0.01), and lean mass compared to

vehicle (Day 0: 26.3 ± 0.7 g vs. Day 14: 24.4 ± 0.6; P<0.001; Fig.6c, e, S6a). A combination of rapamycin and leptin also failed to alter food intake, body weight or glucose tolerance in the POMC-dTA animals (Fig. S6d, e, g, h, i). A summary table for these findings is provided (Fig. S7).

The receptor for α-MSH is MC4R, a G-protein coupled receptor, and *mc4r-/-* mice develop obesity as do patients with mutations in this gene (Fig. S6b) [31]. At baseline, *mc4r-/-* animals were hyperphagic, obese and did not respond to leptin treatment (Fig. S6b, j, k). Similar to POMC-dTA mice, rapamycin did not reduce food intake in *mc4r-/-* mice (Fig. 6g) and while it induced a small decrease in body weight (-5.0 ± 2.1 % vs. 4.5 ± 2.4 %; p<0.001), this was attributable to loss of lean mass (RAP: from 26.5 ± 0.7 g to 24.5 ± 0.6 g; p<0.0001 vs. VEH: from 26.0 ± 0.4 to 25.8 ± 0.4 g) with no effect on fat mass (Fig. 6h-j, S6b). A combination of rapamycin and leptin resulted in a greater reduction of weight and fat mass in the chow-fed WT controls compared to the *mc4r-/-* mutants (Fig. S6m, n).

We also controlled for possible dietary effects by feeding *mc4r-/-* mice a HFD. The *mc4r-/-* mice on a HFD were more obese that DIO mice so we additionally normalized the weight of *mc4r-/-* mice to control DIO animals by feeding them 10% fewer calories than were consumed by ad libitum DIO animals (Fig. 6k, S6c). We refer to these *mc4r-/-* animals as being 'pair-fat' and at 18 weeks, these and the DIO control mice weighed similar amounts. Both groups were then fed ad libitum while being treated with rapamycin for 14 days followed by another 14 days of vehicle treatment. (Fig. 6k). Despite starting from the same baseline weight, rapamycin-treated *mc4r-/-* mice consumed more food than the rapamycin-treated DIO control mice (*mc4r-/-* 50.6 ± 2.9 g vs. DIO 27.4 ± 0.9 g; p<0.01) and even gained weight during the treatment, while, as above, the rapamycin-treated DIO mice showed reduced food intake and body weight (*mc4r -/-* : +10.1 ± 2.2 % vs. DIO : -10.8 ± 0.7 %; p<0.001) (Fig. 6l, m). After 14 days, fat mass was significantly higher in rapamycin-treated *mc4r-/-* mice than in the DIO controls (Fig. 6n. *mc4r -/-*: 52.3 ± 1.1 % vs. DIO: 41.6 ± 0.6 %; p<0.0001), while lean mass did not change (Fig. 6o). Following the cessation of rapamycin treatment, DIO mice showed a significant rebound of food intake and weight and returned to their baseline levels while there was no change in the *mc4r-/-* mice (Fig. 6p, q). A summary table for these findings is provided (Fig. S7). Thus the studies of POMC-ablated and *mc4r-/-* mice show that, similar to *ob/ob* and *db/db* mice, rapamycin does not reduce food intake or fat mass in obese mice with defects in the leptin-melanocortin axis, indicating that increased mTOR activity in POMC neurons is necessary for leptin resistance. We next tested whether increased mTOR activity in POMC neurons is sufficient to cause leptin resistance.

Genetic Perturbations of mTOR Activity Alter Leptin Sensitivity and Energy Balance.

We examined whether mTOR activation in POMC cells can alter leptin sensitivity by breeding POMC-Cre mice to *Tsc1-flox* mice, leading to a POMC-specific deletion of the *Tsc1* gene. TSC1 encodes an endogenous mTOR inhibitor and *Tsc1* knockout mice have increased mTOR activity in numerous tissues (Fig. 7a). Similar to previous reports [32,33], chow-fed POMC$^{tsc1-/-}$ mice were hyperphagic and obese (Fig. S8a, b, c, d). We then assayed leptin sensitivity in these animals by treating them with vehicle followed by leptin (Fig. 7b). In contrast to the leptin responses in the control mice (POMC$^{tsc1+/-}$ and POMC$^{Tsc1+/+}$), leptin did not reduce food intake or body weight in the POMC$^{tsc1-/-}$ mice (Fig. 7c, d). To control for possible independent effects of the obesity that develops in these mice at baseline, we normalized the weight of the POMC$^{tsc1-/-}$ mice to the control mice by pair-feeding them to chow-fed mice. The pair-fed POMC$^{tsc1-/-}$ mice did not respond to leptin and even gained weight during leptin treatment (POMC$^{tsc1-/-}$ +25.3 ± 5.0 % vs. control -2.5 ± 0.6 %; p<0.0001). Followed by the end of leptin treatment, both pair-fed POMC$^{tsc1-/-}$ and control mice were treated with vehicle. The control group showed a rebound increase in their food consumption (3.9 ± 0.3 g vs. 5.8 ± 0.4 g; p<0.001) and weight, while the POMC$^{tsc1-/-}$ did not (Fig. 7e, f, g).

ob/ob mice are leptin deficient and thus ultra-sensitive to leptin administration. We next tested whether increased mTOR activity in POMC neurons can induce complete or partial leptin resistance in *ob/ob* mice. *ob/ob* animals that carried a POMC-specific knockout of *Tsc1* were generated and at baseline, the *ob/ob*-POMC$^{tsc1-/-}$ double-knockout (referred to hereafter as OB-POMC$^{tsc1-/-}$) mice showed a slight increase of lean mass and body weight compared to *ob/ob* controls (OB-control) (Fig. 7k, l, S8i) though the adiposity was similar between the two groups (Fig. 7l). We treated both groups with exogenous leptin for four weeks. In contrast to the OB-control mice, OB-POMC$^{tsc1-/-}$ showed a diminished response to leptin, characterized by 37% greater food consumption (Fig. 7i. 94.0 ± 9.7 g vs. 68.4 ± 4.0 g; $p<0.0001$), 59% higher fat mass (Fig. 7l, m. 27.1 ± 2.5 % vs. 11.2 ± 1.4 %; $p<0.0001$), and reduced weight loss than the OB-controls treated with leptin (Fig. 7k. -26.5 ± 4.2 % vs. -41.7 ± 1.3 %; $p<0.0001$). We next tested whether rapamycin can reverse this partial leptin resistance by treating both groups with rapamycin alone or with rapamycin plus exogenous leptin. Rapamycin alone had no effect on fat mass in the absence of leptin, while the addition of rapamycin to leptin normalized the leptin response of OB-POMC$^{tsc1-/-}$ mice with comparable reductions in food intake (96.6 ± 22.2 g vs. 74.9 ± 7.6 g), body weight (-31.9 ± 4.4 % vs. -37.2 ± 3.3 %) and fat mass (37.4 ± 4.7 % vs. 33.78 ± 4.5 %) compared to the OB-Control group (Fig. 7n-q, S8j).

In a final set of studies, we evaluated whether mutations that blunt the activation of mTOR reduce weight gain in mice fed a HFD. Leucine and methionine activate mTOR and sensing of amino acids is mediated by the GATOR2 complex, while the RHEB GTPase directly activates the mTOR kinase and is inhibited by TSC1 (Fig. S10a) [34-37]. POMC-specific knockouts of *Rheb* and *Wdr24*, were generated by delivering guide RNAs for these two genes, as well as control guide RNAs, into the ARC of POMC-Cas9 mice. The food intake and body weight of these groups was recorded in mice fed a chow diet for three weeks followed by a HFD for three weeks (Fig. S10b). POMC-specific knockouts of *Wdr24* or *Rheb* did not alter food intake or body weight in mice fed a chow diet (Fig. S10c, d), while both groups showed attenuated food intake and weight gain when fed a HFD (Fig. S10e, f). Thus, consistent with the pharmacologic effects of mTOR inhibition by rapamycin, CRISPR-mediated knockouts of these mTOR activators significantly attenuates the development of diet-induced obesity.

Discussion

Obese humans and DIO mice have increased circulating leptin levels and a diminished response to the exogenous hormone [3,7,8]. These are the hallmarks of a hormone resistance syndrome, analogous to insulin resistance as a cause of Type 2 Diabetes [38], thus suggesting that obesity in DIO mice and the general human population is caused by a 'block' in hormone action. The anatomic and molecular basis of this 'block' is unknown and its elucidation would have important implications for the pathogenesis of obesity as well as potential therapeutic applications. In an initial metabolomic screen for biomarkers indicative of a leptin response, we found that the levels of several mTOR ligands inversely correlate with leptin sensitivity leading us to test whether increased mTOR activity might contribute to leptin resistance. We found that rapamycin, a specific mTOR inhibitor, reduces body weight by restoring leptin signaling in DIO mice but not in mice with defects in leptin signaling. We then employed snRNA-seq to show that rapamycin treatment of DIO, but not lean mice, specifically induced genes in POMC neurons that promote leptin signaling and melanocortin production. Further studies showed that POMC neurons and melanocortin signaling are necessary for rapamycin's weight reducing effects and that increased mTOR activity in POMC neurons is sufficient to cause leptin resistance. Thus, while the pathogenesis of insulin resistance is still not completely understood despite many decades of research, these data establish a cellular and molecular basis for leptin resistance in diet-induced obesity in mice. A therapeutic response in DIO mice is highly predictive of a similar response in humans and the pathogenesis of obesity in these animals is considered equivalent to that of obese humans.

Our finding that the leptin resistance that develops in DIO mice is a result of mTOR activation primarily in POMC neurons is consistent with many previous genetic studies of obesity in mice and humans [30,31,39]. POMC encodes a protein precursor that is processed by proteases PCSK1/2 to generate α-MSH which can potently reduce food intake and body weight through broadly distributed receptors in the brain, including MC4R [40,41]. Mutations in *Pomc*, *Pcsk1* and *Mc4r* all cause severe early onset obesity in humans [31,39], and setmelanotide, a peptide analogue of α-MSH, reduces weight in these individuals as well as in patients with leptin receptor mutations [42,43].

Our data indicate that defects in melanocortin signaling can also be acquired when mice are fed a high fat diet. It is not yet clear why this diet leads to increased mTOR activity in POMC neurons but a previous study has suggested that sustained hyperleptinemia can cause leptin resistance [44-46]. We hypothesize that weight gain after consumption of a palatable diet by C57Bl/6J and other strains that are obesity prone leads to increased leptin levels in turn increasing mTOR activity as a means for blunting the response (i.e; tachyphylaxis), as has also been suggested for other hormones including insulin [38].

The activity of POMC neurons is modulated by leptin, insulin, GLP1 and multiple other signals and recent studies have indicated that there is heterogeneity of POMC neurons with different clusters expressing distinct molecular markers [21-23,25,47,48]. Our data revealed that rapamycin affects the POMC subtype that expresses *Lepr*+, with little effect on the other subtypes including a *Pomc+/Htr2c+* cluster. This is consistent with prior results showing that a POMC-specific deletion of *Htr2c* has only minimal effects on body weight in chow fed mice [49], while a deletion of *Lepr* in POMC neurons leads to obesity [50]. While an earlier report suggested that rapamycin blunted the acute effects of leptin, this study only evaluated the effect of a single dose of leptin on food intake [51]. It is thus possible that while transient mTOR activation is required for leptin's acute effects, chronic mTOR activation, possibly induced by chronically high hormone levels, leads to a down regulation of leptin signaling. Consistent with this, our studies as well as prior studies of mice with a deletion of *Tsc1* in POMC neurons, revealed that increased mTOR activity in these neurons causes obesity and that rapamycin can reduce adiposity in these as well as in aged obese mice [32,33]. However, this previous study of aged mice

did not show that the ability of rapamycin to reduce weight was a result of a restoration of leptin signaling *in vivo* nor did it establish the importance of mTOR hyperactivity in POMC neurons as a cause of diet-induced obesity the pathogenesis of which, as mentioned, is considered to be equivalent human obesity.

Our results are also consistent with numerous prior reports showing that rapamycin treatment or diets low in methionine or leucine mitigate diet-induced obesity [52-54]. However, in these prior studies, an effect on leptin sensitivity was not evaluated and the role of POMC neurons in mediating this response was not shown. Indeed, we find that downregulation of the leucine-sensing mTORC1 pathway in POMC neurons blunts weight gain in POMC-*Wdr24* knockout mice fed a HFD. Thus overall, our data unify and extend a large number of prior studies by showing that increased mTOR signaling in POMC neurons is both necessary and sufficient for the development of diet-induced obesity and provides a mechanism explaining how and why low protein diets and rapamycin reduce the obesity of DIO mice.

We also found that increased mTOR activity in POMC neurons of *ob/ob*-POMC$^{tsc1-/-}$ mice leads to partial leptin resistance in *ob/ob* mice, which are normally extremely sensitive to leptin. However, leptin's effect, while reduced, is still significant in these mice suggesting that the hormone acts on other target populations including AGRP neurons, an arcuate population that drives appetite and is inhibited by leptin. Our finding that DIO is caused by defects in POMC neurons is consistent with the fact that *ob/ob* mice are significantly more obese than DIO mice, likely as a result of leptin action at other sites besides POMC neurons. However, these data do not exclude the possibility that mTOR might also affect leptin signaling in additional cell types. Consistent with this, we observed increased pS6 levels in a number of hypothalamic sites outside the ARC in DIO vs. chow fed mice such as the ventromedial hypothalamus, preoptic areas, the basomedial amygdala and striatum. It is not clear which of these neurons express the leptin receptor and their possible contributions to leptin resistance awaits further investigation.

The gene expression data suggest that chronic mTOR activation activates genes that diminish leptin signaling and that rapamycin reverses this. Our finding that rapamycin increases the levels of pSTAT3 provides one of several potential mechanisms by which leptin signaling is restored, possibly achieved by decreasing the expression of *Ptprm* and *Ptprt*, which dephosphorylate pStat3 , A role for mTOR activation to increase expression of pStat3 phosphatases had not been shown previously. However other mechanisms in addition to dephosphorylation of pStat3 may also contribute because a POMC-specific knockout of *Stat3* results in only a mild obese phenotype [5,55]. Other signaling molecules have also been shown to contribute to leptin resistance including SOC3 and PIAS proteins that inhibit JAK and STAT activity respectively which also decrease leptin signal transduction [55-62]. Another report suggested that increased mTOR signaling in POMC neurons increases the activity of an inhibitory K^{ATP} channel and that POMC neurons from POMC$^{tsc1-/-}$ mice are hyperpolarized via increased K^{ATP} conductance [32]. Other reports also show that increased levels of PIP3 can silence POMC neurons by increasing K^{ATP} channel activity [63]. Thus increased expression of this or similar channels could also reduce the activity of POMC subtype 2 neurons expressing the leptin receptor. Recent reports have further suggested that a knockout of *Grb10*, an endogenous mTOR inhibitor, in POMC neurons enhances leptin signaling [4,64] but, similar to the minimal effects of a POMC knockout of *Lepr* and *Stat3*, a POMC-specific knockout of this gene did not alter the weight of chow-fed mice to the same extent as a knockout of *Tsc1* in our and the aforementioned studies [32,33]. Inhibiting HDAC6 has also been reported to alleviate leptin resistance though in this case the effect appeared to be peripheral, possibly leading to alterations of signaling onto POMC neurons to alter mTOR activity [65]. In addition, prior reports have suggested that impaired autophagy and/or increased ER stress in POMC neurons can cause leptin resistance [66,67], though the metabolic impairment seen in mice with mutations in *Atg7* in POMC neurons did not lead to the same level of obesity that develops in DIO mice or mice with a POMC deletion of *Tsc1* [67]. Still other studies have suggested that ER stress

contributes to leptin resistance which can be alleviated by the drug celastrol and while a possible role for the IL1 receptor was shown [68-72], its precise cellular target is unknown. Further studies will thus be necessary to integrate these findings and fully establish whether mTOR affects these and other signaling pathways to regulate leptin sensitivity.

Rapamycin was first developed clinically as an immune suppressor [73,74]. More recently it is being evaluated as a possible agent for extending lifespan but the mechanism responsible for the potential effects on longevity are not fully understood [75]. Increased BMI has been shown to be an independent risk factor for mortality [76], raising the possibility that restored leptin sensitivity and reduced body weight could contribute to rapamycin's effect on longevity. However, rapamycin also leads to glucose intolerance and insulin resistance which would generally limit its utility, especially in obese patients with prediabetes and diabetes [16,73,74]. We also found that, while not worsening diabetes, rapamycin treatment of DIO mice has only a marginal effect to improve glucose metabolism in DIO mice. It seems likely that the benefit of weight loss is counteracted by the negative effect of rapamycin on insulin signaling. Consistent with this, we found that co-administration of rapamycin and leptin significantly blunted glucose intolerance in wild-type mice but not in mice with defects in melanocortin signaling. This is consistent with prior studies showing that leptin further improves glucose tolerance in mice with mutations in *Akt* and that POMC neurons control glucose metabolism in addition to maintaining body weight [20,67,77-79].

While rapamycin specifically reduced fat mass in animals with intact leptin signaling, we also observed highly reproducible effects of rapamycin to significantly decrease lean mass in animals with defects in leptin and melanocortin signaling. The mechanism accounting for this effect is unknown though we also found that rapamycin elicited a modest effect to increase energy expenditure in DIO mice. However the effects on lean mass in DIO mice with functional leptin signaling were minimal and significantly smaller than the effect on fat mass, consistent with numerous prior reports showing that leptin specifically reduces fat mass with no effect on lean mass in leptin-sensitive animals [2,3]. Thus, the effect of rapamycin on lean mass is likely to be independent of leptin via a yet unknown mechanism. Prior reports have shown that an adipose-tissue knockout of *Raptor*, a component of mTORC1, prevents weight gain of animals fed on HFD [80], while an adipose-tissue knockout of *Rictor*, a component of mTORC2, exacerbates weight gain on HFD [81]. However, these studies did not evaluate effects on lean mass, and it is possible that rapamycin might also have other effects on this or other tissues including alterations of muscle mass.

Overall, these data suggest that selective inhibition of mTOR in POMC neurons could provide a new strategy for leptin re-sensitization as a treatment for obesity. While several new incretin-based therapies have shown potent effects on reversing obesity, it is likely that other therapeutic approaches will be necessary for managing obesity in patients who cannot tolerate these drugs, fail to respond or to help maintain weight in patients after treatment [82,83]. There is also significant recidivism after weight loss post bariatric surgery which further highlights the need to develop means for weight management [84]. Leptin levels decrease after weight loss and some of the weight gain that is seen after bariatric surgery or dieting appears to be a result of this [85]. Thus, new therapies that enhance endogenous leptin sensitivity via cell-type-specific inhibition of mTOR activity may provide an important therapeutic modality on its own or as an adjunct to incretin therapies or bariatric surgery.

In addition to the effect of mTOR on leptin signaling, altered mTOR function has also been linked to a broad spectrum of psychiatric diseases, including addiction, depression, Parkinson's disease, and autism. Chronic alterations of mTOR activity have been shown to alter neuronal sensitivity to other neuromodulators such as dopamine, serotonin and their mimetics [86-90]. Recent advances in developing brain-specific rapalogues provide an entry point to selectively reduce mTOR activity specifically in brain [91]. Thus, the development of new technologies for cell specific delivery of rapamycin or delineating cell-type-specific mTOR

interactomes in diseases associated with cell specific increases of mTOR activity could provide new avenues for treating many diseases [92].

In summary, we show that leptin resistance in DIO animals is caused by increased mTOR activity in POMC neurons, and that rapamycin reduces obesity by re-sensitizing endogenous leptin signaling in these cells. These findings thus have important implications for the pathogenesis of obesity and potential therapeutic applications.

Author contributions

B.T. designed and conducted the experiments, analyzed the data, conceptualized the results, wrote the manuscript and provided the funding support. K.H. designed and conducted the experiments, breeded mouse models, wrote the manuscript and conceptualized the results. L.K. conducted electrophysiological recordings and analysis. J.D.L. conducted quality control and initial analysis of single-nucleus RNAseq datasets. Z.Z. conducted metabolomic and lipidomic sample preparation and analysis. J.D.R. provided resources for metabolomics and lipidomics. J.M.F. conceived and led the study, wrote the manuscript and conceptualized the results, provided resources and funding support.

Acknowledgements

We thank Cori Bargmann and Nat Heintz for their advice throughout the project and their critical comments on the manuscript. We thank Donghoon Lee for the help with tissue dissections. We thank Alexandre Moura Assis for their help with feeding animals and proofreading the manuscript. We thank Lisa Pomeranz, Max Halaas for feeding animals. We thank Xianfeng Zeng and Wenyun Lu for assisting Z.Z. to perform sample preparation, lipidomics analysis and develop the LC methods. We thank Connie Zhao and Hong Duan for their help with 10X genomics library preparation and sequencing. B.T. acknowledges support from the David Rockefeller Fellowship. J.M.F. acknowledges support from the JPB foundation. B.T. and K.H. acknowledge support from the Robertson Therapeutic Development Fund, and the clinical and translational science awards.

Methods

Animals

Wild-type mice (#000664), *db/db* mice (#000697), *mc4r-/-* (#032518), POMC-cre (#005965) *Tsc1 fl/fl* (#005680), AgRP-cre (#012899), LSL-Cas9 (#026175) were acquired from Jackson Lab and *ob/ob* were F1, bred in lab, from a cross between male *ob/ob* and female *ob/+* (#000632). All crosses were bred in lab from the above animals. Animals were kept at ambient temperature and humidity-controlled housing with a 12hr light-dark cycle and on a standard-chow diet (PicoLab® Rodent Diet 205053) unless otherwise indicated. Diet-induced-obese (DIO) wild-type mice were fed on high-fat diet (HFD, Research Diets, Cat# D12492, Rodent Diet With 60 kcal% Fat) starting at ~6 weeks old and used for experiments starting at 24 weeks old (fed on HFD for at least 18 weeks). Aged wild-type mice (~15 months old, #000664) were acquired from Jackson Lab. All experiments were conducted according to AAALAC approved animal protocols #18050, #18051, #22012 and #21064.

Plasma metabolomics and lipidomics

Wildtype animals (Jackson #000664) were fed either chow (PicoLab® Rodent Diet 205053) or high fat diet (HFD, Research Diets cat. #D12492 Rodent Diet With 60 kcal% Fat) starting at 8-9 weeks of age. *ob/ob* males, bred in lab as described above, were also fed either chow or HFD and pairfed to their wildtype counterparts. Food intake for the wildtype animals were measured weekly, divided by 7, and then fed in that amount daily to the pairfed *ob/ob* animals for 18 weeks. Despite this pairfeeding scheme, the *ob/ob* animals gained more food than their wildtype counterparts. After 18 weeks of daily pairfeeding, all animals were i.p. injected with PBS (Gibco, Cat# 14190-144) at 12 hour intervals for 24hrs and blood was collected and processed as described below in section (7). Following 5 days of recovery, the animals were i.p. injected with 12.5 mg/kg leptin, dissolved in PBS at 12 hour intervals for 24hrs and blood was again collected. (1) Metabolomics. For polar metabolites, 10ul of serum was extracted with 40ul MeOH pre-cooled on dry ice. After vertexing, samples are left on dry ice for 5min then centrifuged at 16,000 X g for 10 min at 4°C. Supernatant was subjected to LC-MS analysis. Positive and Negative mode of metabolomics were run on a quadrupole-orbitrap mass spectrometer (Q Exactive, Thermo Fisher Scientific, San Jose, CA) coupled with hydrophilic interaction chromatography (HILIC) via electrospray ionization. LC separation was done with a XBridge BEH Amide column (2.1 mm x 150 mm x 2.5 mm particle size, 130 A □ pore size; Waters, Milford, MA) using a gradient of solvent A (20 mM ammonium acetate, 20 mM ammounium hydroxide in95:5 water:acetonitrile, pH 9.45) and solvent B (acetonitrile). Flow rate was 150 mL/min. The LC gradient was: 0 min, 85% B;2 min, 85% B; 3 min, 80% B; 5 min, 80% B; 6 min, 75% B; 7 min, 75% B; 8 min, 70% B; 9 min, 70% B; 10 min, 50% B; 12 min,50% B; 13 min, 25% B; 16 min, 25% B; 18 min, 0% B; 23 min, 0% B; 24 min, 85% B. Injection volume was 5ul for all serum samples at the autosampler temperature of 5 ^{o}C. (2) Lipidomics. Serum lipidomic samples are extracted with ethyl acetate. Serum (4µl) was added to ethyl acetate (100µl) and centrifuged 16,000 X g for 10min, and the supernatant was collected. The same process was repeated, and supernatant is combined. The resulting extract was dried down and redissolved in 1:1:1 methanol:acetonitrile:2-propanol (200µl) before analysis by Q Exactive Plus mass spectrometer coupled to a Vanquish UHPLC system (Thermo Fisher Scientific) using positive and negative-mode electrospray ionization. The LC separation was achieved on an Agilent Poroshell 120 EC-C18 column (150 × 2.1mm, 2.7 µm particle size) at a flow rate of 150 µl min^{-1}. The gradient was 0minutes, 25% B; 2minutes, 25% B; 4minutes, 65% B; 16minutes, 100% B; 20minutes, 100% B; 21minutes, 25% B; 27minutes, 25% B. Solvent A is 1mM ammonium acetate + 0.2% acetic acid in water:methanol (90:10). Solvent B is 1mM ammonium acetate + 0.2% acetic acid in methanol:2-propanol (2:98).

Pharmacological administration
Recombinant mouse leptin (R&D 498-OB-05M) was dissolved in PBS and injected intraperitoneally (i.p.) or delivered via a subcutaneous osmotic pump (Alzet Cat# 2002, 2004, or 2006). Osmotic pumps were filled and calibrated using the manufacturer's instructions. They were inserted dorsally under the skin of an isoflurane-anesthetized mouse using sterile surgery techniques. Rapamycin (LC Laboratories, Cat# 53123-88-9) was first dissolved in DMSO at 200 mg/ml, then diluted in 5% PEG 400 and 5% Tween 80 (in PBS) to a final concentration of 0.5 mg/ml. I.p. injections were done at indicated concentrations using insulin syringes (Beckton Dickinson, Cat# 324911).

Magnetic resonance imaging (MRI)
Body fat mass was measured by MRI using Echo-MRI 100H (EchoMRI, LL). Body fat percentage was calculated by dividing fat mass over total body mass. Lean mass was calculated by subtracting fat mass from total body mass.

Leptin sensitivity test
Animals were administered with leptin (at indicated doses) or PBS either by i.p. injections every 12 hours or via osmotic pumps implanted 1 day prior to the start of the experiment. Food intake and body weight were measured through the course of treatment as indicated.

Glucose tolerance test
Animals fasted overnight were i.p. injected 5-20% glucose dissolved in PBS as indicated. Total amount of glucose injected was based on lean mass times the dosage. Dosage used for each experiment and cohort was indicated in the manuscript. Blood glucose in the GTT assay and adlibitum-fed conditions were measured by tail vein sampling using a Breeze2 glucometer (Bayer SKU: breeze2meter UPC: 301931440010). For the GTT in DIO mice, the groups of mice receiving 600 ng/hr leptin were i.p. injected 1 mg/kg leptin 1 hour prior to the glucose injection, while the other groups of mice were i.p. injected PBS 1 hour prior to the GTT started.

Leptin ELISA
Blood was collected retro-orbitally using EDTA coated capillaries (Drummond Calibrated Micropipettes Glass Capillaries with EDTA 100µl, Cat# 2-000-100-D). Samples were spun for 20 minutes at 4°C and supernatant collected as plasma and frozen immediately in liquid nitrogen and stored at -80°C in screw cap tubes. Plasma leptin was measured by ELISA (Alpco, Cat# 22-LEPMS-E01) according to the manufacturer's protocol.

Pairfeeding or Pairfat conditions
Pairfeeding was conducted by measuring the daily or weekly food intake of the group which shows lower food intake and feeding that same amount to the other group. In some conditions where the group being pairfed still weighs significantly higher than the group it is pairfed to, we further restricted their food intake 10% lower than the amount of food they received in order to reach equal body weight (Pairfat) as the other group before the subsequent tests. Animals were single housed during experiments. Food intake and body weight were measured daily or weekly using an Ohaus Scale.

Whole-brain mTOR activity (pS6) mapping
SHIELD-based whole-brain clearing and labeling was employed for mapping pS6 activity in DIO mice and chow fed mice. Mice ad libitum fed on HFD or chow were anesthetized with isoflurane and transcardially perfused with PBS containing 10 U/ml heparin, followed by 4% PFA. The dissected brains were fixed in 4% PFA for 24 h at 4 °C. Brains were then transferred to PBS containing 0.1% sodium azide until brain clearing and labeling. Brains were processed by

LifeCanvas Technologies following the SHIELD protocol as previously published [18,93]. Samples were cleared for 7 days with Clear+ delipidation buffer, followed by batch labeling in SmartBatch+ with and 5 µg anti-Rabbit pS6 (Invitrogen Cat# 44-923G) per brain. Fluorescently conjugated secondary antibodies were applied in 1:2 primary/secondary molar ratios (Jackson ImmunoResearch). Labeled samples were incubated in EasyIndex (LifeCanvas Technologies) for refractive index matching (n = 1.52) and imaged with SmartSPIM (LifeCanvas Technologies) at 4 µm z-step and 1.8 µm xy pixel size. Image analysis was conducted following the procedures as previously published [18,93].

Single-nucleus RNA sequencing

Animals received 3-day treatment of rapamycin and/or leptin were anesthetized under 5% isoflurane 4-hour post last injection. ARC was microdissected under a stereo microscope in pre-chilled dissection buffer and immediately transferred to dry ice prior to downstream nuclei extraction at the same day. After dissection, frozen tissues on dry ice were immediately transferred to Teflon homogenizer containing 1 ml pre-chilled NP40 lysis buffer (Fisher Cat# FNN0021) and homogenized for 15-30 times using a pellet pestle on ice. Homogenized samples were incubated for another 10-15 min on ice, followed by passing through a 70 µm Flowmi Cell Strainer and a 40 µm Flowmi Cell Strainer (Millipore Sigma). The collected flowthrough was centrifuged at 500-1000 rcf for 5 min at 4°C and pellets were resuspended in staining buffer. 30% iodixanol buffer was then carefully loaded at the bottom of resuspended nuclei at 4°C. Samples were centrifuged at 10000 rcf for 20 min at 4°C. Supernatant containing debris was carefully removed. Pellets were resuspended in staining buffer containing anti-NeuN Alexa 647 antibody (abcam, Cat# ab190565) and HashTag antibodies (1 µl for labeling ~1 x 10^6 nuclei, BioLegend, TotalSeqB anti-Nuclear Pore) in order to enrich neurons and multiplex samples. After antibody incubation and rotating for 30 min at 4°C, samples were washed with staining buffer without antibodies for 3 times. Samples were resuspended in FACS buffer after last-round wash and sent for FACS sorting. Hoechst 33342 (ThermoFisher Scientific, Cat# H3570) were added at a final concentration of 0.2 mM to label nuclei. Sorted nuclei were sent for downstream 10X genomics 3' RNA-seq with feature barcode library preparation and sequenced using NovaSeq sequencer or DNBseq sequencer at BGI with ~30000 reads/nuclei on average. Dissection buffer contains 1X HBSS, 2.5 mM HEPES-KOH [pH 7.4], 35 mM Glucose, 4 mM $NaHCO_3$, and Actinomycin D (Sigma-Aldrich, Cat# A1410) at a final concentration of 20 µg/ml. NP40 lysis buffer contains 10 mM Tris-HCl [pH 7.4], 10 mM NaCl, 3 mM $MgCl_2$, 0.1% NP40 dissolved in nuclease-free water. For 1 ml NP40 lysis buffer, 1 µl DTT, 25 µl 20 U/µl SupeRasine (Thermo Cat# AM2696), 12.5 µl 40 U/ µl RNasin (Promega Cat# N2615), 10 µl protease and phosphatase inhibitor cocktail (100X; Thermo Cat# 78442), 40 µl 1 mg/ml Actinomycin D were added right before use. 30% iodixanol buffer contains 0.25M sucrose, 25mM KCl, 5mM $MgCl_2$, 20mM Tricine-HCl [pH 8.0] and 30% Iodixanol dissolved in nuclease-free water. DTT, Superasine, Rnasin and protease inhibitors were added at the same concentration as NP40 lysis buffer right before use. Staining buffer contains 2% BSA, 0.05% NP40 dissolved in nuclease-free 1X PBS. Superasine, Rnasin and protease inhibitors were added at the same concentration as NP40 lysis buffer right before use. FACS buffer contains 2% BSA dissolved in nuclease-free 1X PBS buffer. Superasine, Rnasin and protease inhibitors were added at the same concentration as NP40 lysis buffer right before use.

snRNA-seq analysis

The fastq files were aligned to mouse genome (mm10), and the expression levels in each cell were estimated with Cellranger (v 6.0.0). The gene expression count matrix for each sample was processed with the following steps: (1) Estimate doublet with Scrublet (https://github.com/swolock/scrublet) [94]; (2) Estimate and correct the ambient RNA

contaminations with SoupX (https://github.com/constantAmateur/SoupX) [95]; (3) Load the corrected counting matrix into Seurat object with log normalization; (4) Calculate the proportion of UMIs from mitochondrial genes; (5) Demultiplex with hashtag oligos followed the Seurat vignette (https://satijalab.org/seurat/articles/hashing_vignette.html); (6) The cells assigned as doublets or mitochondrial content greater than 1% were removed. The Seurat objects were integrated by following the RPCA workflow (https://satijalab.org/seurat/articles/integration_rpca.html) [96]. The number of PCs used for UMAP calculation was selected with elbow plot [97]. Then, the clustering was calculated with Leiden algorithm [98]. To select the optimized resolution, the resolution was tested from 0.1 to 1.0 and was selected with clustree. The Chow_HFD was assigned as the reference dataset. The clustering information were mapped and transferred from the reference to OB_RAP_VEH datasets by following the Seurat vignette (https://satijalab.org/seurat/articles/integration_mapping.html).
The differential gene expression of each comparison was performed with Seurat::FindMarkers() with logfc.threshold greater than 0.14, and raw p values were corrected using p.adjust() with the 'BH' method. Significant differential expression genes were defined as log2 (Fold Change) greater than 0.26 or less than -0.26, and corrected p values less than 0.05.

Histology

Mice were transcardially perfused with PBS (Fisher, Cat# BP39920) followed by 4% paraformaldehyde (PFA, EMS Cat# 15714-S). Brains were dissected and post-fixed in 4% PFA at 4°C overnight. Brains were sectioned into 50-µm coronal slices using a vibratome (Leica). For immunohistochemistry, brain sections were blocked (0.1% Triton X-100 (Thermo Cat# 85111) in PBS, 3% bovine serum albumin (Sigma Cat# A9647-500G), 2% normal donkey serum (Jackson ImmunoResearch Cat# 017-000-121)). For pSTAT3 staining, sections were first rinsed in 1% H2O2 + 1% NaOH in H2O for 20 min, at room temperature, then transferred to 0.3% glycine in 1X PBS for 10 min, at room temperature prior to blocking. Sections post blocking were then incubated with primary antibody (rabbit anti-Phospho-S6, Invitrogen, Cat# 44-923G, 1:1000 dilution; rabbit anti Phosphp-Stat3, Cell Signaling, Cat# 9145 1:500 dilution; chicken anti GFP, 1:1000 dilution, abcam, Cat# ab13970) for 2 days at 4°C. Sections were then washed and incubated with secondary antibody (donkey anti-chicken IgG Alexa 488, Jackson Immunoresearch, Cat# 703-546-155, 1:1000 dilution; donkey anti-rabbit IgG Alexa 594, Invitrogen, Cat# A21207, 1:500 or 1:1000 dilution) for 1 hour at room temperature, washed again, mounted with DAPI Fluoromount-G (Southern Biotech Cat# 0100-20) and imaged with SlideView microscope (VS200, Olympus). Images underwent minimal processing (such as adjusting brightness and contrast) performed using ImageJ. The CellCounter plugin for ImageJ was used to quantify numbers and percentages of co-localizations from sections.

Slice preparation and electrophysiology

Acute coronal hypothalamic brain slices (200 µm) were prepared from POMC-eGFP (5-64 weeks old) mice fed either on chow diet, or high fat diet for a minimum of 16 weeks. Mice were anesthetized with isoflurane prior to decapitation and removal of the entire brain which was immediately submerged in ice-cold 'slicing' solution containing (in mM): 85 NaCl, 2.5 KCl, 0.5 CaCl2, 4 MgCl2, 25 NaHCO3, 1.25 NaH2PO4, 64 sucrose, 25 glucose. This solution was bubbled with 95% O2 and 5% CO2, pH 7.4. Coronal hypothalamic slices (200µm) were made with a moving blade microtome (VT1000S, Leica). The slices were kept at 32 °C for 40 min in recording solution containing (in mM) 125 NaCl, 2.5 KCl, 1.25 NaH2PO4, 26 NaHCO3, 10 glucose, 2 CaCl2 and 1 MgCl2, pH 7.4 when bubbled with 95% O2 and 5% CO2 before being kept at room temperature prior to recording. Cell-attached patch-clamp recordings were made in voltage clamp configuration with 0pA holding current at room temperature from

eGFP-expressing neurons in the arcuate nucleus. Neurons were visualized using epifluorescence and patched under DIC imaging on an upright microscope (Zeiss Axioskop 2FS Plus) equipped with a CCD camera (Hamamatsu). Patch pipettes pulled (Narishige PP-830) from borosilicate glass (Sutter Instrument) had tip resistances of 7–11 MΩ and were filled with K-gluconate internal containing (in mM): 135 potassium gluconate, 4 KCl, 0.05 EGTA, 10 Hepes, 4 MgATP, 10 Na-Phosphocreatine, pH adjusted to 7.3 with KOH, 290 OSM. All chemicals were obtained from Sigma. Leptin stock was prepared in PBS (1mg/ml or 100µM), then diluted in ASCF (100nM) and bath applied for 20 minutes via perfusion. Recordings were acquired with an Axopatch 200B amplifier, filtered to 2 kHz and digitized at 10 kHz (pClamp10 software, Molecular Devices). Data were analyzed using IGOR Pro (Wavemetrics) and NeuroMatic (http://www.neuromatic.thinkrandom.com/). Mean firing rate was detected in 10 second bins and maximum firing rate was recorded in each condition. Baseline firing rate was calculated in the first minute of recording, ASCF was calculated in the minute before peptide application. Neurons were considered excited or inhibited by leptin if firing changed more than 10%. For i.p. injections DIO mice fed on high fat diet for more than 16 weeks were injected either with rapamycin (2 mg/kg) or vehicle once a day for 3 consecutive days before brain slice preparation.

Viral injections into the ARC

Cre-inducible AAV5-hsyn-DIO-mCherry (Addgene Cat# 50459-AAV5) and AAV5-mCherry-flex-dtA (plasmid was obtained from Addgene Cat# 58536, AAV viruses were packaged at Janelia Research Campus) viruses were injected into ARC of POMC-Cre+ animals using stereotactic surgery as follows: Mice were anesthetized with 3% isoflurane in oxygen, placed in a stereotaxic apparatus (Kopf Instruments) and kept at 1.5% isoflurane during surgery. Viruses were bilaterally delivered using a borosilicate glass pipette connected to Nanoject (Drummond, Cat# 3-000-203-G/X) in ARC (200 nl per coordinate, 50 nl/min). The coordinates to locate ARC were relative to the bregma: AP/DV/ML = −1.75/−5.95/±0.25 mm, AP/DV/ML = −1.75/−5.75/±0.25 mm. After finishing injection at each coordinate, syringes were held at the coordinate for another 3 minutes. Animals were allowed to recover (and adjust eating habits) for 8 weeks post-surgery, before being used in experiments. Plasmids containing guide-RNAs were designed, customized and generated at VectorBuilder. Plasmids were then packaged into AAV viruses at Janelia Research Campus.

Metabolic cages

Diet-induced obese mice were singly housed in a climate-controlled (temperature: 22 °C; humidity: 55%; 12-hour light–12-hour dark cycle) automated home cage phenotyping system (TSE) with ad libitum access to water and high-fat-diet. After 7 days of adaptation to the TSE cage, receiving daily mock IP injections, the mice were treated daily with IP vehicle or IP 2 mg/kg Rapamycin for 6 days (Fig. S4). Data were collected and analyzed as recommended by the manufacturers. Energy expenditure and respiratory exchange ratio (RER) were measured by an indirect gas calorimetry module recording open circuit oxygen consumption and carbon dioxide production (VO_2 and VCO_2). Locomotor activity was recorded as beam breaks converted into distance/velocity, measuring activity in three dimensions and analyzed in the metabolic cage using custom software. Statistical assessment of the data was conducted using CalR software (https://www.calrapp.org).

Statistics and reproducibility

We conducted statistical analyses using GraphPad Prism 9.0. Throughout the paper, values were reported as mean ± SEM (error bar). Each statistical test performed was denoted in the figure legends. P-values for pair-wise comparisons were obtained using two-tailed student's t-test. P-values for two independent group comparisons were either obtained using two-tailed

student's t-test or nonparametric Mann-Whitney test based on data distributions. P-values for multiple group comparisons were conducted using one-way or two-way ANOVA (with repeated measures when possible) based on the number of factors and corrected for multiple comparisons using Fisher's LSD test, Tukey's test or Sidak's test, indicated in the figure legends. The experiments were not randomized. Data for each experiment were repeated with at least two different cohorts. Representative trial data or pooled data from multiple cohorts were used for conducting statistics and plotting figures. The investigators were not blinded to allocation during experiments and outcome assessments.

Methods references

1. Davoudian, P.A., L.X. Shao, and A.C. Kwan, *Shared and Distinct Brain Regions Targeted for Immediate Early Gene Expression by Ketamine and Psilocybin.* ACS Chem Neurosci, 2023. **14**(3): p. 468-480.
2. Park, Y.G., et al., *Protection of tissue physicochemical properties using polyfunctional crosslinkers.* Nat Biotechnol, 2018.
3. Wolock, S.L., R. Lopez, and A.M. Klein, *Scrublet: Computational Identification of Cell Doublets in Single-Cell Transcriptomic Data.* Cell Syst, 2019. **8**(4): p. 281-291 e9.
4. Young, M.D. and S. Behjati, *SoupX removes ambient RNA contamination from droplet-based single-cell RNA sequencing data.* Gigascience, 2020. **9**(12).
5. Stuart, T., et al., *Comprehensive Integration of Single-Cell Data.* Cell, 2019. **177**(7): p. 1888-1902 e21.
6. Becht, E., et al., *Dimensionality reduction for visualizing single-cell data using UMAP.* Nat Biotechnol, 2018.
7. Traag, V.A., L. Waltman, and N.J. van Eck, *From Louvain to Leiden: guaranteeing well-connected communities.* Sci Rep, 2019. **9**(1): p. 5233.

References

1 The Lancet Gastroenterology, H. Obesity: another ongoing pandemic. *Lancet Gastroenterol Hepatol* **6**, 411 (2021). https://doi.org:10.1016/S2468-1253(21)00143-6

2 Halaas, J. L. *et al.* Weight-reducing effects of the plasma protein encoded by the obese gene. *Science* **269**, 543-546 (1995). https://doi.org:10.1126/science.7624777

3 Halaas, J. L. *et al.* Physiological response to long-term peripheral and central leptin infusion in lean and obese mice. *Proc Natl Acad Sci U S A* **94**, 8878-8883 (1997). https://doi.org:10.1073/pnas.94.16.8878

4 Liu, H. *et al.* Hypothalamic Grb10 enhances leptin signalling and promotes weight loss. *Nat Metab* **5**, 147-164 (2023). https://doi.org:10.1038/s42255-022-00701-x

5 Xu, A. W., Ste-Marie, L., Kaelin, C. B. & Barsh, G. S. Inactivation of signal transducer and activator of transcription 3 in proopiomelanocortin (Pomc) neurons causes decreased pomc expression, mild obesity, and defects in compensatory refeeding. *Endocrinology* **148**, 72-80 (2007). https://doi.org:10.1210/en.2006-1119

6 Cowley, M. A. *et al.* Leptin activates anorexigenic POMC neurons through a neural network in the arcuate nucleus. *Nature* **411**, 480-484 (2001). https://doi.org:10.1038/35078085

7 Maffei, M. *et al.* Leptin levels in human and rodent: measurement of plasma leptin and ob RNA in obese and weight-reduced subjects. *Nat Med* **1**, 1155-1161 (1995). https://doi.org:10.1038/nm1195-1155

8 Heymsfield, S. B. *et al.* Recombinant leptin for weight loss in obese and lean adults: a randomized, controlled, dose-escalation trial. *JAMA* **282**, 1568-1575 (1999). https://doi.org:10.1001/jama.282.16.1568

9 Christoffersen, B. O. *et al.* Beyond appetite regulation: Targeting energy expenditure, fat oxidation, and lean mass preservation for sustainable weight loss. *Obesity (Silver Spring)* **30**, 841-857 (2022). https://doi.org:10.1002/oby.23374

10 Lawler, K. *et al.* Leptin-Mediated Changes in the Human Metabolome. *J Clin Endocrinol Metab* **105**, 2541-2552 (2020). https://doi.org:10.1210/clinem/dgaa251

11 Wolfson, R. L. *et al.* Sestrin2 is a leucine sensor for the mTORC1 pathway. *Science* **351**, 43-48 (2016). https://doi.org:10.1126/science.aab2674

12 Gu, X. *et al.* SAMTOR is an S-adenosylmethionine sensor for the mTORC1 pathway. *Science* **358**, 813-818 (2017). https://doi.org:10.1126/science.aao3265

13 Laplante, M. & Sabatini, D. M. An emerging role of mTOR in lipid biosynthesis. *Curr Biol* **19**, R1046-1052 (2009). https://doi.org:10.1016/j.cub.2009.09.058

14 Ham, D. J. *et al.* The neuromuscular junction is a focal point of mTORC1 signaling in sarcopenia. *Nat Commun* **11**, 4510 (2020). https://doi.org:10.1038/s41467-020-18140-1

15 Jacobson, L. Middle-aged C57BL/6 mice have impaired responses to leptin that are not improved by calorie restriction. *Am J Physiol Endocrinol Metab* **282**, E786-793 (2002). https://doi.org:10.1152/ajpendo.00495.2001

16 Kocalis, H. E. *et al.* Rictor/mTORC2 facilitates central regulation of energy and glucose homeostasis. *Mol Metab* **3**, 394-407 (2014). https://doi.org:10.1016/j.molmet.2014.01.014

17 Kamohara, S., Burcelin, R., Halaas, J. L., Friedman, J. M. & Charron, M. J. Acute stimulation of glucose metabolism in mice by leptin treatment. *Nature* **389**, 374-377 (1997). https://doi.org:10.1038/38717
18 Park, Y. G. *et al.* Protection of tissue physicochemical properties using polyfunctional crosslinkers. *Nat Biotechnol* (2018). https://doi.org:10.1038/nbt.4281
19 Friedman, J. M. Leptin and the endocrine control of energy balance. *Nat Metab* **1**, 754-764 (2019). https://doi.org:10.1038/s42255-019-0095-y
20 Xu, J. *et al.* Genetic identification of leptin neural circuits in energy and glucose homeostases. *Nature* **556**, 505-509 (2018). https://doi.org:10.1038/s41586-018-0049-7
21 Campbell, J. N. *et al.* A molecular census of arcuate hypothalamus and median eminence cell types. *Nat Neurosci* **20**, 484-496 (2017). https://doi.org:10.1038/nn.4495
22 Biglari, N. *et al.* Functionally distinct POMC-expressing neuron subpopulations in hypothalamus revealed by intersectional targeting. *Nat Neurosci* **24**, 913-929 (2021). https://doi.org:10.1038/s41593-021-00854-0
23 Deng, G. *et al.* Single-Nucleus RNA Sequencing of the Hypothalamic Arcuate Nucleus of C57BL/6J Mice After Prolonged Diet-Induced Obesity. *Hypertension* **76**, 589-597 (2020). https://doi.org:10.1161/HYPERTENSIONAHA.120.15137
24 Saucisse, N. *et al.* Functional heterogeneity of POMC neurons relies on mTORC1 signaling. *Cell Rep* **37**, 109800 (2021). https://doi.org:10.1016/j.celrep.2021.109800
25 Steuernagel, L. *et al.* HypoMap-a unified single-cell gene expression atlas of the murine hypothalamus. *Nat Metab* **4**, 1402-1419 (2022). https://doi.org:10.1038/s42255-022-00657-y
26 Zhang, X. *et al.* Identification of STAT3 as a substrate of receptor protein tyrosine phosphatase T. *Proc Natl Acad Sci U S A* **104**, 4060-4064 (2007). https://doi.org:10.1073/pnas.0611665104
27 Pei, Z. *et al.* Gabra5 plays a sexually dimorphic role in POMC neuron activity and glucose balance. *Front Endocrinol (Lausanne)* **13**, 889122 (2022). https://doi.org:10.3389/fendo.2022.889122
28 Vong, L. *et al.* Leptin action on GABAergic neurons prevents obesity and reduces inhibitory tone to POMC neurons. *Neuron* **71**, 142-154 (2011). https://doi.org:10.1016/j.neuron.2011.05.028
29 Paeger, L. *et al.* Energy imbalance alters Ca(2+) handling and excitability of POMC neurons. *Elife* **6** (2017). https://doi.org:10.7554/eLife.25641
30 Zhan, C. *et al.* Acute and long-term suppression of feeding behavior by POMC neurons in the brainstem and hypothalamus, respectively. *J Neurosci* **33**, 3624-3632 (2013). https://doi.org:10.1523/JNEUROSCI.2742-12.2013
31 Loos, R. J. *et al.* Common variants near MC4R are associated with fat mass, weight and risk of obesity. *Nat Genet* **40**, 768-775 (2008). https://doi.org:10.1038/ng.140
32 Yang, S. B. *et al.* Rapamycin ameliorates age-dependent obesity associated with increased mTOR signaling in hypothalamic POMC neurons. *Neuron* **75**, 425-436 (2012). https://doi.org:10.1016/j.neuron.2012.03.043
33 Mori, H. *et al.* Critical role for hypothalamic mTOR activity in energy balance. *Cell Metab* **9**, 362-374 (2009). https://doi.org:10.1016/j.cmet.2009.03.005

34 Valenstein, M. L. *et al.* Structure of the nutrient-sensing hub GATOR2. *Nature* **607**, 610-616 (2022). https://doi.org:10.1038/s41586-022-04939-z
35 Cai, W., Wei, Y., Jarnik, M., Reich, J. & Lilly, M. A. The GATOR2 Component Wdr24 Regulates TORC1 Activity and Lysosome Function. *PLoS Genet* **12**, e1006036 (2016). https://doi.org:10.1371/journal.pgen.1006036
36 Yang, H. *et al.* Mechanisms of mTORC1 activation by RHEB and inhibition by PRAS40. *Nature* **552**, 368-373 (2017). https://doi.org:10.1038/nature25023
37 Inoki, K., Li, Y., Xu, T. & Guan, K. L. Rheb GTPase is a direct target of TSC2 GAP activity and regulates mTOR signaling. *Genes Dev* **17**, 1829-1834 (2003). https://doi.org:10.1101/gad.1110003
38 Shanik, M. H. *et al.* Insulin resistance and hyperinsulinemia: is hyperinsulinemia the cart or the horse? *Diabetes Care* **31 Suppl 2**, S262-268 (2008). https://doi.org:10.2337/dc08-s264
39 Frank, G. R. *et al.* Severe obesity and diabetes insipidus in a patient with PCSK1 deficiency. *Mol Genet Metab* **110**, 191-194 (2013). https://doi.org:10.1016/j.ymgme.2013.04.005
40 Fenselau, H. *et al.* A rapidly acting glutamatergic ARC-->PVH satiety circuit postsynaptically regulated by alpha-MSH. *Nat Neurosci* **20**, 42-51 (2017). https://doi.org:10.1038/nn.4442
41 Yaswen, L., Diehl, N., Brennan, M. B. & Hochgeschwender, U. Obesity in the mouse model of pro-opiomelanocortin deficiency responds to peripheral melanocortin. *Nat Med* **5**, 1066-1070 (1999). https://doi.org:10.1038/12506
42 Chen, K. Y. *et al.* RM-493, a melanocortin-4 receptor (MC4R) agonist, increases resting energy expenditure in obese individuals. *J Clin Endocrinol Metab* **100**, 1639-1645 (2015). https://doi.org:10.1210/jc.2014-4024
43 Kievit, P. *et al.* Chronic treatment with a melanocortin-4 receptor agonist causes weight loss, reduces insulin resistance, and improves cardiovascular function in diet-induced obese rhesus macaques. *Diabetes* **62**, 490-497 (2013). https://doi.org:10.2337/db12-0598
44 Knight, Z. A., Hannan, K. S., Greenberg, M. L. & Friedman, J. M. Hyperleptinemia is required for the development of leptin resistance. *PLoS One* **5**, e11376 (2010). https://doi.org:10.1371/journal.pone.0011376
45 Zhao, S. *et al.* Partial Leptin Reduction as an Insulin Sensitization and Weight Loss Strategy. *Cell Metab* **30**, 706-719 e706 (2019). https://doi.org:10.1016/j.cmet.2019.08.005
46 Ottaway, N. *et al.* Diet-induced obese mice retain endogenous leptin action. *Cell Metab* **21**, 877-882 (2015). https://doi.org:10.1016/j.cmet.2015.04.015
47 Dodd, G. T. *et al.* Insulin regulates POMC neuronal plasticity to control glucose metabolism. *Elife* **7** (2018). https://doi.org:10.7554/eLife.38704
48 Koch, M. *et al.* Hypothalamic POMC neurons promote cannabinoid-induced feeding. *Nature* **519**, 45-50 (2015). https://doi.org:10.1038/nature14260
49 Berglund, E. D. *et al.* Serotonin 2C receptors in pro-opiomelanocortin neurons regulate energy and glucose homeostasis. *J Clin Invest* **123**, 5061-5070 (2013). https://doi.org:10.1172/JCI70338

50 Balthasar, N. *et al.* Leptin receptor signaling in POMC neurons is required for normal body weight homeostasis. *Neuron* **42**, 983-991 (2004). https://doi.org:10.1016/j.neuron.2004.06.004
51 Cota, D. *et al.* Hypothalamic mTOR signaling regulates food intake. *Science* **312**, 927-930 (2006). https://doi.org:10.1126/science.1124147
52 Wang, L. *et al.* Methionine restriction alleviates high-fat diet-induced obesity: Involvement of diurnal metabolism of lipids and bile acids. *Biochim Biophys Acta Mol Basis Dis* **1866**, 165908 (2020). https://doi.org:10.1016/j.bbadis.2020.165908
53 Zhou, Z. *et al.* A fifty percent leucine-restricted diet reduces fat mass and improves glucose regulation. *Nutr Metab (Lond)* **18**, 34 (2021). https://doi.org:10.1186/s12986-021-00564-1
54 Zhang, Q. *et al.* Leptin signaling is required for leucine deprivation-enhanced energy expenditure. *J Biol Chem* **289**, 1779-1787 (2014). https://doi.org:10.1074/jbc.M113.528943
55 Ernst, M. B. *et al.* Enhanced Stat3 activation in POMC neurons provokes negative feedback inhibition of leptin and insulin signaling in obesity. *J Neurosci* **29**, 11582-11593 (2009). https://doi.org:10.1523/JNEUROSCI.5712-08.2009
56 Pedroso, J. A. *et al.* Inactivation of SOCS3 in leptin receptor-expressing cells protects mice from diet-induced insulin resistance but does not prevent obesity. *Mol Metab* **3**, 608-618 (2014). https://doi.org:10.1016/j.molmet.2014.06.001
57 Olofsson, L. E., Unger, E. K., Cheung, C. C. & Xu, A. W. Modulation of AgRP-neuronal function by SOCS3 as an initiating event in diet-induced hypothalamic leptin resistance. *Proc Natl Acad Sci U S A* **110**, E697-706 (2013). https://doi.org:10.1073/pnas.1218284110
58 Howard, J. K. *et al.* Enhanced leptin sensitivity and attenuation of diet-induced obesity in mice with haploinsufficiency of Socs3. *Nat Med* **10**, 734-738 (2004). https://doi.org:10.1038/nm1072
59 Mori, H. *et al.* Socs3 deficiency in the brain elevates leptin sensitivity and confers resistance to diet-induced obesity. *Nat Med* **10**, 739-743 (2004). https://doi.org:10.1038/nm1071
60 Bjorbak, C. *et al.* SOCS3 mediates feedback inhibition of the leptin receptor via Tyr985. *J Biol Chem* **275**, 40649-40657 (2000). https://doi.org:10.1074/jbc.M007577200
61 Bence, K. K. *et al.* Neuronal PTP1B regulates body weight, adiposity and leptin action. *Nat Med* **12**, 917-924 (2006). https://doi.org:10.1038/nm1435
62 Cheng, A. *et al.* Attenuation of leptin action and regulation of obesity by protein tyrosine phosphatase 1B. *Dev Cell* **2**, 497-503 (2002). https://doi.org:10.1016/s1534-5807(02)00149-1
63 Plum, L. *et al.* Enhanced PIP3 signaling in POMC neurons causes KATP channel activation and leads to diet-sensitive obesity. *J Clin Invest* **116**, 1886-1901 (2006). https://doi.org:10.1172/JCI27123
64 Yu, Y. *et al.* Phosphoproteomic analysis identifies Grb10 as an mTORC1 substrate that negatively regulates insulin signaling. *Science* **332**, 1322-1326 (2011). https://doi.org:10.1126/science.1199484

65 Cakir, I. *et al.* Histone deacetylase 6 inhibition restores leptin sensitivity and reduces obesity. *Nat Metab* **4**, 44-59 (2022). https://doi.org:10.1038/s42255-021-00515-3
66 Park, S., Aintablian, A., Coupe, B. & Bouret, S. G. The endoplasmic reticulum stress-autophagy pathway controls hypothalamic development and energy balance regulation in leptin-deficient neonates. *Nat Commun* **11**, 1914 (2020). https://doi.org:10.1038/s41467-020-15624-y
67 Coupe, B. *et al.* Loss of autophagy in pro-opiomelanocortin neurons perturbs axon growth and causes metabolic dysregulation. *Cell Metab* **15**, 247-255 (2012). https://doi.org:10.1016/j.cmet.2011.12.016
68 Schneeberger, M. *et al.* Mitofusin 2 in POMC neurons connects ER stress with leptin resistance and energy imbalance. *Cell* **155**, 172-187 (2013). https://doi.org:10.1016/j.cell.2013.09.003
69 Ozcan, L. *et al.* Endoplasmic reticulum stress plays a central role in development of leptin resistance. *Cell Metab* **9**, 35-51 (2009). https://doi.org:10.1016/j.cmet.2008.12.004
70 Feng, X. *et al.* IL1R1 is required for celastrol's leptin-sensitization and antiobesity effects. *Nat Med* **25**, 575-582 (2019). https://doi.org:10.1038/s41591-019-0358-x
71 Lee, J. *et al.* Withaferin A is a leptin sensitizer with strong antidiabetic properties in mice. *Nat Med* **22**, 1023-1032 (2016). https://doi.org:10.1038/nm.4145
72 Liu, J., Lee, J., Salazar Hernandez, M. A., Mazitschek, R. & Ozcan, U. Treatment of obesity with celastrol. *Cell* **161**, 999-1011 (2015). https://doi.org:10.1016/j.cell.2015.05.011
73 Saxton, R. A. & Sabatini, D. M. mTOR Signaling in Growth, Metabolism, and Disease. *Cell* **168**, 960-976 (2017). https://doi.org:10.1016/j.cell.2017.02.004
74 Wullschleger, S., Loewith, R. & Hall, M. N. TOR signaling in growth and metabolism. *Cell* **124**, 471-484 (2006). https://doi.org:10.1016/j.cell.2006.01.016
75 Harrison, D. E. *et al.* Rapamycin fed late in life extends lifespan in genetically heterogeneous mice. *Nature* **460**, 392-395 (2009). https://doi.org:10.1038/nature08221
76 Global, B. M. I. M. C. *et al.* Body-mass index and all-cause mortality: individual-participant-data meta-analysis of 239 prospective studies in four continents. *Lancet* **388**, 776-786 (2016). https://doi.org:10.1016/S0140-6736(16)30175-1
77 Hay, N. Akt isoforms and glucose homeostasis - the leptin connection. *Trends Endocrinol Metab* **22**, 66-73 (2011). https://doi.org:10.1016/j.tem.2010.09.003
78 Chen, W. S. *et al.* Leptin deficiency and beta-cell dysfunction underlie type 2 diabetes in compound Akt knockout mice. *Mol Cell Biol* **29**, 3151-3162 (2009). https://doi.org:10.1128/MCB.01792-08
79 Parton, L. E. *et al.* Glucose sensing by POMC neurons regulates glucose homeostasis and is impaired in obesity. *Nature* **449**, 228-232 (2007). https://doi.org:10.1038/nature06098
80 Polak, P. *et al.* Adipose-specific knockout of raptor results in lean mice with enhanced mitochondrial respiration. *Cell Metab* **8**, 399-410 (2008). https://doi.org:10.1016/j.cmet.2008.09.003
81 Cybulski, N., Polak, P., Auwerx, J., Ruegg, M. A. & Hall, M. N. mTOR complex 2 in adipose tissue negatively controls whole-body growth. *Proc Natl Acad Sci U S A* **106**, 9902-9907 (2009). https://doi.org:10.1073/pnas.0811321106
82 Wilding, J. P. H. *et al.* Once-Weekly Semaglutide in Adults with Overweight or Obesity. *N Engl J Med* **384**, 989-1002 (2021). https://doi.org:10.1056/NEJMoa2032183

83 Jastreboff, A. M. *et al.* Tirzepatide Once Weekly for the Treatment of Obesity. *N Engl J Med* **387**, 205-216 (2022). https://doi.org:10.1056/NEJMoa2206038
84 Magro, D. O. *et al.* Long-term weight regain after gastric bypass: a 5-year prospective study. *Obes Surg* **18**, 648-651 (2008). https://doi.org:10.1007/s11695-007-9265-1
85 Terra, X. *et al.* Long-term changes in leptin, chemerin and ghrelin levels following different bariatric surgery procedures: Roux-en-Y gastric bypass and sleeve gastrectomy. *Obes Surg* **23**, 1790-1798 (2013). https://doi.org:10.1007/s11695-013-1033-9
86 Wang, X. *et al.* Nucleus accumbens core mammalian target of rapamycin signaling pathway is critical for cue-induced reinstatement of cocaine seeking in rats. *J Neurosci* **30**, 12632-12641 (2010). https://doi.org:10.1523/JNEUROSCI.1264-10.2010
87 Abdallah, C. G. *et al.* Modulation of the antidepressant effects of ketamine by the mTORC1 inhibitor rapamycin. *Neuropsychopharmacology* **45**, 990-997 (2020). https://doi.org:10.1038/s41386-020-0644-9
88 Li, N. *et al.* mTOR-dependent synapse formation underlies the rapid antidepressant effects of NMDA antagonists. *Science* **329**, 959-964 (2010). https://doi.org:10.1126/science.1190287
89 Santini, E., Heiman, M., Greengard, P., Valjent, E. & Fisone, G. Inhibition of mTOR signaling in Parkinson's disease prevents L-DOPA-induced dyskinesia. *Sci Signal* **2**, ra36 (2009). https://doi.org:10.1126/scisignal.2000308
90 Tang, G. *et al.* Loss of mTOR-dependent macroautophagy causes autistic-like synaptic pruning deficits. *Neuron* **83**, 1131-1143 (2014). https://doi.org:10.1016/j.neuron.2014.07.040
91 Zhang, Z. *et al.* Brain-restricted mTOR inhibition with binary pharmacology. *Nature* **609**, 822-828 (2022). https://doi.org:10.1038/s41586-022-05213-y
92 Branon, T. C. *et al.* Efficient proximity labeling in living cells and organisms with TurboID. *Nat Biotechnol* **36**, 880-887 (2018). https://doi.org:10.1038/nbt.4201
93 Davoudian, P. A., Shao, L. X. & Kwan, A. C. Shared and Distinct Brain Regions Targeted for Immediate Early Gene Expression by Ketamine and Psilocybin. *ACS Chem Neurosci* **14**, 468-480 (2023). https://doi.org:10.1021/acschemneuro.2c00637
94 Wolock, S. L., Lopez, R. & Klein, A. M. Scrublet: Computational Identification of Cell Doublets in Single-Cell Transcriptomic Data. *Cell Syst* **8**, 281-291 e289 (2019). https://doi.org:10.1016/j.cels.2018.11.005
95 Young, M. D. & Behjati, S. SoupX removes ambient RNA contamination from droplet-based single-cell RNA sequencing data. *Gigascience* **9** (2020). https://doi.org:10.1093/gigascience/giaa151
96 Stuart, T. *et al.* Comprehensive Integration of Single-Cell Data. *Cell* **177**, 1888-1902 e1821 (2019). https://doi.org:10.1016/j.cell.2019.05.031
97 Becht, E. *et al.* Dimensionality reduction for visualizing single-cell data using UMAP. *Nat Biotechnol* (2018). https://doi.org:10.1038/nbt.4314
98 Traag, V. A., Waltman, L. & van Eck, N. J. From Louvain to Leiden: guaranteeing well-connected communities. *Sci Rep* **9**, 5233 (2019). https://doi.org:10.1038/s41598-019-41695-z

Figure Legends

Fig 1. Metabolomic and lipidomic profiling of plasma metabolites associated with leptin resistance. (**a**) Schematic of *ob/ob* (OB) animals pairfed to WT animals daily for 18 weeks fed on chow or HFD. At 19 weeks, mice were i.p. injected with vehicle (VEH) every 12 hours for 24 hours followed by blood collection. At 20 weeks, mice were i.p. injected with 12.5 mg/kg leptin (LEP) every 12 hours for 24 hours followed by blood collection. (**b**) Time-course percentage of body weight relative to starting point (week 0), (**c**) Cumulative calories consumed (kcal) of WT mice fed on chow vs. HFD over 18 weeks. (Two-way ANOVA, with Tukey's multiple comparisons, n=6, 6, 9, 10 for WT-Chow, WT-DIO, OB-Chow, OB-HFD; respectively). (**d**) Comparisons of 24-hour food intake (g), 24-hour % weight change, and body temperature post VEH vs. post LEP (Two-way ANOVA, with Fisher's LSD comparisons, n=6, 6, 9, 10 for WT-Chow, WT-DIO, OB-Chow, OB-HFD respectively). (**e**) Heatmap of the cluster of metabolites levels higher in DIO post LEP vs. VEH. Z-score scale at bottom right. Comparisons of representative metabolites levels (ion count) post VEH vs. post LEP: (**g**) Leucine, (**f**) TG_NH4(56:6), (**h**) PA (48:0) and (**i**) Glucosyl ceramide (d18:1/22:0). (Two-way ANOVA, with Fisher's LSD comparisons; n=6 for WT-Chow, n=6, 7 for DIO that received VEH vs. LEP, n=9 for OB-Chow, n=10 for OB-HFD). All error bars represent mean ± SEM. ns, not significant, *P < 0.05, **P < 0.01, ***P < 0.001, ****P < 0.0001. Additional information is included in Fig. S1.

Fig 2. Rapamycin reduces obesity in DIO mice and potentiates exogenous leptin in chow-fed lean mice but not in *ob/ob* or *db/db* mice. WT-DIO Prolonged treatment: (**a**) Cumulative food intake (g) and (**b**) Weight (%), (**c**) Fat mass (%), (**d**) Lean mass (g) in DIO mice that received daily 2 mg/kg i.p. rapamycin (RAP) or i.p. vehicle (VEH) for 10 weeks (n=8, 10 respectively; Two-way ANOVA, with Šidák's multiple comparisons). WT-DIO: DIO mice receivied RAP or VEH daily for 14 days (**e**) Cumulative food intake (g) and (**f**) Weight (%) (**g**) Fat mass (%) and (**h**) Lean mass (g). (n=11; two-way ANOVA, with Šidák's multiple comparisons). WT-Chow: (**i**) Cumulative food intake (g) and (**j**) Weight (%) (**k**) Fat mass (%) and (**l**) Lean mass (g) at day 14 in chow-fed lean mice that received daily RAP plus 600 ng/hr leptin (LEP), RAP plus VEH, LEP plus VEH, VEH plus VEH (n=12, 14, 14, 13 respectively; two-way ANOVA with Tukey's multiple comparisons for cumulative food intake and weight; one-way ANOVA with Tukey's multiple comparisons for comparisons of fat mass and lean mass). OB-Chow: (**m**) Cumulative food intake (g) and (**n**) Weight (%), (**o**) Fat mass (%) and (**p**) Lean mass (g) at day 14 in chow-fed *ob/ob* mice that received RAP plus 300 ng/hr leptin (LEP), RAP plus VEH, VEH plus LEP, VEH plus VEH (n=5, 9, 7, 8, respectively; two-way ANOVA with Tukey's multiple comparisons for cumulative food intake and weight; one-way ANOVA with Tukey's multiple comparisons for fat mass and lean mass). DB-Chow**:** (**q**) Cumulative food intake (g) and (**r**) Weight (%), (**s**) Fat mass (%) and (**t**) Lean mass (g) at day 0 and day 14 in chow-fed *db/db* mice that received RAP vs. VEH (n=8, 5 respectively; two-way ANOVA, with Šidák's multiple comparisons). All error bars represent mean ± SEM. ns, not significant, *P < 0.05, **P < 0.01, ***P < 0.001, ****P < 0.0001. Additional information is included in Fig. S2 and S3.

Fig 3. Rapamycin increases the sensitivity of exogenous leptin in DIO mice, and exogenous leptin mitigates rapamycin-induced hyperglycemia. (**a**) Schematic of DIO mice that received daily i.p. injections of 2 mg/kg Rapamycin (RAP) vs. vehicle (VEH) followed by a leptin sensitivity test. Each group received i.p. injections of 2 mg/kg leptin (LEP) twice a day for 3 days followed by i.p. injections of vehicle (VEH) twice a day for 3 days. (**b**) Plasma leptin in DIO mice after receiving 3-week RAP vs. VEH prior to a leptin sensitivity test (n=16, 14, respectively; two-tailed Student's t-tests). (**c**) Cumulative food intake (g) and (**d**) Weight (%) during leptin sensitivity test where RAP or VEH-treated DIO mice received VEH vs. LEP (n=8, 8 for each group; two-way ANOVA, with Šidák's multiple comparisons). (**e**) Schematic of DIO mice

that received daily i.p. injections of RAP vs. VEH. The group of mice that received VEH were pairfed to the group of mice that received RAP for 5 weeks. Leptin sensitivity test was conducted after 5-week treatment and daily pair-feeding. For the leptin sensitivity test, each group of mice received i.p. injections of 2 mg/kg LEP twice daily for 3 days followed by i.p. injections of VEH twice daily for 3 days. Both groups of mice had adlibitum access to food during the test. See also Fig. S4a, b. (**f**) Plasma leptin in DIO mice after receiving 3-week RAP vs. Pairfed-VEH prior to leptin sensitivity test (n=6, 6 for each group; two-tailed Student's t-tests). (**g**) Cumulative food intake (g) and (**h**) Weight (%) of RAP vs. pairfed VEH-treated DIO mice received LEP (n=6, 6; two-tailed Mann-Whitney tests). Adlibitum glucose levels in the WT-Chow (**i**), WT-DIO (**j**), OB-Chow (**k**), DB-Chow (**l**) groups shown in Fig 2. at day 5-7 while receiving daily RAP+LEP, RAP, LEP, VEH treatment. (WT-Chow: n=10, 8, 11, 10 for each group; WT-DIO: n=17, 18, 17, 16 for each group; OB-Chow: n=7, 6, 6, 5 for each group; one-way ANOVA, with Holm-Šidák's multiple comparisons. DB-Chow: n=8, 7 for each group; two-tailed Student's t tests.). (**m**) Time-course of glucose levels from glucose tolerance test (GTT) in WT-Chow mice receiving RAP plus 600 ng/hr LEP, RAP plus VEH, LEP plus VEH or VEH plus VEH for 7 days and (**n**) quantification of the area under curve (n=10, 10, 10, 9, respectively; one-way ANOVA, with Holm-Šidák's multiple comparisons). (**o**) Time-course of glucose levels in GTT in DIO mice that received RAP plus 600 ng/hr LEP, RAP plus VEH, LEP plus VEH and VEH plus VEH for 3 weeks and (**p**) quantification of the area under curve (n=5, 6, 4, 4, respectively; one-way ANOVA, with Holm-Šidák's multiple comparisons). All error bars represent mean ± SEM. ns, not significant, *P < 0.05, **P < 0.01, ***P < 0.001, ****P < 0.0001. Additional information is included in Fig. S4.

Fig 4. Single-nucleus RNA sequencing identifies hypothalamic POMC neurons primarily responding to rapamycin in a leptin-signaling-dependent manner. (**a**) Immunohistochemical staining of pS6 levels, and DAPI, in DIO mice compared to chow-fed lean mice. (**b**) Quantification of pS6 densities in DIO mice compared to chow-fed lean mice (n=9 sections from 3 mice for each group, two-tailed Mann-Whitney tests). (**c**) Schematic of chow-fed lean mice or DIO mice followed by 3-day daily i.p. injections of 2 mg/kg RAP vs. VEH. 4-hour after last treatment, ARC tissues wre microdissected for snRNA-seq with integrated analysis across groups. (**d**) UMAP representations of 18 clusters of cell types identified and shared across all Lean-RAP, Lean-VEH, DIO-RAP, DIO-VEH groups (n = 4934, 5182, 5992, 4514 nuclei profiled from the ARC for each group). (**e**) Violin Plot depicting the expressions levels of enriched molecular markers for each cluster. (**f, g**) Quantification of total numbers of regulated genes by RAP vs. VEH across unsupervised clusters and canonical cell types. (**h**) A heatmap representing the enriched molecular markers for POMC subtypes that are shared across all groups. (**i, j**) Volcano plots showing differentially expressed genes in POMC subtypes in response to RAP vs. VEH between Lean and DIO groups. (**k**) Immunohistochemical staining of pS6 and POMC-GFP levels in DIOs that received 3-day RAP vs. VEH treatment, followed by acute leptin treatment (2 mg/kg, i.p. injections). Quantification of co-localization of pS6 and POMC-GFP (n=5 sections from 3 mice for each group, two-tailed Mann-Whitney tests). (**l**) Immunohistochemical staining of pSTAT3 and POMC-GFP levels in DIOs that received 3-day RAP vs. VEH treatment, followed by acute leptin treatment (2 mg/kg, i.p. injections). Quantification of co-localization of pSTAT3 and POMC-GFP (n=5 sections from 3 mice for each group, two-tailed Mann-Whitney tests). All error bars represent mean ± SEM. ns, not significant, *P < 0.05, **P < 0.01, ***P < 0.001, ****P < 0.0001. Additional information is included in Fig. S5.

Fig 5. Rapamycin increases baseline firing rate and proportion of leptin-excited POMC neurons in DIO mice. (**a**) Example traces of cell-attached recordings from POMC-eGFP neurons at baseline (in ASCF). Example trace from a chow-fed mouse, DIO mouse, a DIO mouse with 3-day vehicle injection and from a DIO mouse with 3-day rapamycin injection (top to

bottom). Scale bar represents 50 pA for chow and DIO mice, 100 pA for vehicle treated mice and 20 pA for rapamycin treated mice and 2 seconds for all traces. (**b**) Baseline firing rate is significantly decreased in DIO mice and is rescued with rapamycin. Summary data showing individual and mean values for baseline firing rate (Hz) of POMC neurons from recorded from chow-fed, DIO mice, DIO mice with 3-day vehicle treatment and DIO mice with 3-day rapamycin treatment (left to right) (orange box represents i.p. injection). Baseline firing rate is significantly decreased in DIO mice (0.91 ± 0.11 Hz, n = 154; p = 0.007) and DIO mice with treated with vehicle (0.81 ± 0.20 Hz, n = 36; p = 0.003) compared to chow fed mice (2.00 ± 0.42 Hz, n = 51). Rapamycin treatment significantly rescues decreased firing rate in DIO mice (2.75 ± 0.64 Hz, n = 28) both compared to DIO mice with no treatment (p<0.0001) and DIO mice with treated with vehicle (p = 0.0004, all Mann-Whitney tests). (**c**) Proportion of spiking POMC neurons in chow-fed mice, DIO mice, DIO mice with 3-day vehicle treatment and DIO mice with 3-day rapamycin treatment (top to bottom). Percentage of spiking POMC neurons is significantly decreased in DIO mice (57.80%, n = 154) and DIO mice treated with vehicle (47.22%, n = 36) compared to chow fed mice (90.20% n = 51; both p<0.0001, two tailed binomial test). Rapamycin treatment significantly increases proportion of spiking POMC neurons (82.14%, n = 28) compared to DIO mice (p = 0.012) and DIO vehicle-treated (p<0.0001, both binomial test). (**d**) Example traces cell-attached recordings from POMC-eGFP neurons in bath-applied leptin (100 nM, 20 mins). Example trace from a chow-fed mouse, DIO mouse with low firing a DIO mouse with 3-day vehicle injection and example trace from a DIO mouse with 3-day rapamycin injection (top to bottom). Scale bar represents 50 pA for chow and DIO mice, 100pA for vehicle treated mice and 20 pA for rapamycin treated mice and 2 seconds for all traces. (**e**) Summary data showing individual and mean POMC firing rates (Hz) in ASCF and bath-applied leptin (100 nM, 20 mins) recorded from chow-fed, DIO mice, DIO mice with 3-day vehicle treatment and DIO mice with 3-day rapamycin treatment (left to right, orange box represents i.p. injection). Leptin significantly increases firing rate in POMC neurons in chow-fed mice from 2.95 ± 0.34 to 4.41 ± 1.31 Hz (n = 20; p = 0.028), in DIO mice from 1.50 ± 0.29 to 1.77 ± 0.33 Hz (n = 50; p = 0.0238) and in DIO mice with 3-day rapamycin treatment from 3.58 ± 0.88 to 4.81 ± 1.03 Hz (n = 17, p = 0.0208). Mean firing rate of POMC neurons of DIO mice with 3-day vehicle treatment does not significantly change in the presence of leptin 1.38 ± 0.31 vs 1.87 ± 0.67 Hz (n = 18; p = 0.6095, all Wilcoxon matched pairs). Mean firing rate in leptin is significantly higher in POMC neurons of rapamycin-treated DIO mice 4.81 ± 1.03 Hz (n = 17) compared to vehicle treated DIO mice 1.87 ± 0.67 Hz (n = 18; p=0.0047) and untreated DIO mice 1.77 ± 0.33 Hz (n = 50; p = 0.0002, both Mann-Whitney test). (**f**) Rapamycin significantly increases proportion of leptin-excited neurons in DIO mice. The proportion of leptin-excited POMC neurons in chow-fed mice 60% (n = 20), DIO mice 52% (n = 50), DIO mice with vehicle treatment 50% (n = 18) and DIO with 3-day rapamycin treatment 76.5% (n = 17) (from top to bottom). Rapamycin significantly increases the proportion of leptin-excited neurons in DIO mice 76.5% (n = 17) compared to DIO mice treated with vehicle (p = 0.0148, two-tailed binomial test).

Fig 6. Rapamycin minimally regulates food intake, weight and adiposity in obese mice models deficient in melanocortin signaling. (**a**) POMC-ablation: Schematic of POMC-dTA vs. POMC-mCherry mice that received daily i.p. injections of 2 mg/kg RAP vs. VEH for 14 days and diagram of the interaction between the mTOR and POMC neurons. (**b**) Cumulative food intake (g) and (**c**) Weight (%) over 14-day treatment, (**d**) Fat mass (%) and (**e**) Lean mass (g) at Day 0 vs. Day 14 of POMC-dTA vs. POMC-mCherry mice receiving RAP vs. VEH (n=10 for RAP in POMC-dTA, n=12 for VEH in POMC-dTA, n=8 for RAP in POMC-mCherry, n = 8 for VEH in POMC-mCherry; two-way ANOVA with Tukey's multiple comparisons tests). (**f**) MC4R knockout: Schematic of *mc4r-/-* mice on chow that received RAP vs. VEH for 14 days and diagram of the interaction between the mTOR and POMC-MC4R pathway. (**g**) Cumulative food intake (g), (**h**) Weight (%) in *mc4r-/-* mice, (**i**) Fat mass (%) and (**j**) Lean mass (g) at Day 0 vs. Day 14 of *mc4r-*

/- that received RAP vs. VEH (n=8, 10, respectively; two-way ANOVA, with Šidák's multiple comparisons). (**k**) Schematic of the study design: *mc4r-/-* mice on HFD pairfat to WT-DIO mice for 16 weeks, after which they received 14 -days of daily 2 mg/kg RAP i.p. injections followed by 14-day daily i.p. VEH injections. Both groups of mice had adlibitum access to HFD throughout the pharmacological treatment. Schematic diagram of testing diet-dependent effects of rapamycin in *mc4r-/-* obese mice. (**l**) Cumulative food intake (g) and (**m**) Weight (%), (**n**) Fat mass (%) and (**o**) Lean mass (g) at Day 0 and Day 14 in pairfat *mc4r-/-* and WT-DIO mice that received daily RAP for 14 days while adlibitum fed on HFD. (**p**) Averaged daily food intake and (**q**) Change in weight (%) in (previously pairfat) *mc4r-/-* vs. WT-DIO mice after withdrawal from RAP while receiving VEH for 14 days (n=7 for pairfat *mc4r-/-* mice, n=6 for WT-DIO mice, two-way ANOVA, with Šidák's multiple comparisons). All error bars represent mean ± SEM. ns, not significant, *P < 0.05, **P < 0.01, ***P < 0.001, ****P < 0.0001. Additional information is included in Fig. S6 and S7.

Fig 7. Genetic upregulation of mTOR activity in POMC cells causes leptin resistance, which can be reversed by rapamycin. (**a**) Diagram illustrates the deletion of the *tsc1* gene, resulting in mTOR activation in POMC cells and subsequent development of obesity. (**b**) Schematic depicting the leptin-sensitivity test in POMC$^{tsc1-/-}$ and WT mice fed on chow. Both mice received twice-daily i.p. injections of VEH for 3 days, followed by twice-daily i.p injections of 0.5 mg/kg LEP for 3 days. (**c**) Averaged daily food intake (g) and (**d**) Change in weight (%) during the 3-day leptin-sensitivity test in POMC$^{tsc1-/-}$ vs. WT mice ad libitum fed on chow (n=10 for POMC$^{tsc1-/-}$ mice, n=12 for WT control mice; two-way ANOVA, with Šidák's multiple comparisons). (**e**) Schematic depicting leptin-sensitivity test in pairfat POMC$^{tsc1-/-}$ and WT mice fed chow. Both groups received twice-daily i.p. injections of 0.5 mg/kg LEP for 3 days, followed by twice-daily i.p injections of VEH for 3 days. Both groups of mice had adlibitum access to food throughout VEH and LEP treatment. (**f**) Averaged daily food intake (g) and (**g**) Change in weight (%) during the 3-day leptin-sensitivity test in POMC$^{tsc1-/-}$ vs. WT mice ad libitum fed on chow (n=5 for POMC$^{tsc1-/-}$ mice, n=11 for WT control mice; two-way ANOVA, with Šidák's multiple comparisons). (**h**) Diagram illustrates a complete loss of leptin signaling in *ob/ob*/POMC$^{tsc1-/-}$ mice. (**i**) Schematic of *ob/ob*/POMC$^{tsc1-/-}$ (OB-POMC$^{tsc1-/-}$) and *ob/ob* controls (OB-control: *ob/ob* POMC-Cre+ *tsc1fl/-* and *ob/ob* POMC-Cre- *tsc1 fl/fl*) mice on chow that received 150 ng/hr LEP or VEH for 4 weeks, followed by an 8-12 week recovery period. After recovery, these mice received 150 ng/hr LEP plus 2mg/kg RAP (i.p. injections 3 times a week) vs. VEH plus 2mg/kg RAP (i.p. injections 3 times a week). (**j**) Cumulative food intake (g) and (**k**) Weight (%) during 4-week LEP treatment, (**l**) Fat mass (%) and (**m**) Lean mass (g) at Week 0 vs. at the end of Week 4 in OB-POMC$^{tsc1-/-}$ vs. OB-control (n=19, 26; respectively; n=4 for VEH in POMC$^{tsc1-/-}$; two-way ANOVA, with Tukey's multiple comparisons). (**n**) Cumulative food intake (g) and (**o**) Weight (%) during 4-week treatment, (**p**) Fat mass (%) and (**q**) Lean mass (g) at Week 0 vs. at the end of Week 4 in OB-POMC$^{tsc1-/-}$ vs. OB-control (n=11 for RAP+LEP in OB-POMC$^{tsc1-/-}$, n=13 for RAP+LEP in OB-control, n=6 for RAP+VEH in OB-POMC$^{tsc1-/-}$, n=13 for RAP+VEH in OB-control; two-way ANOVA with Tukey's multiple comparisons tests). All error bars represent mean ± SEM. ns, not significant, *P < 0.05, **P < 0.01, ***P < 0.001, ****P < 0.0001. Additional information is included in Fig. S8.

Supplementary Figure Legends

Fig S1. Overview of metabolomic and lipidomic plasma profiles in response to leptin across Chow, DIO, OB-Chow and OB-HFD mouse models. (**a**) Heatmap overview of metabolomics and (**b**) DIO-cluster specific lipidomics in WT-Chow, WT-DIO, OB-Chow, and OB-HFD treated with VEH vs. LEP. Comparisons of representative metabolite levels (ion count) post VEH vs. LEP: (**c**) Methionine, (**d**) PG (38:0) (Two-way ANOVA, with Fisher's LSD comparisons,

n = 6 for WT-Chow, n = 6, 7 for DIO receiving VEH vs. LEP, n = 9 for OB-Chow, n = 10 for OB-HFD). (**e**) Weight (g) during 18-week pairfeeding scheme (two-way ANOVA, with Tukey's multiple comparisons, n = 6, 6, 9, 10 for WT-Chow, WT-DIO, OB-Chow, OB-HFD; respectively). (**f**) Weekly consumption of calories (kcal) during 18-week pairfeeding scheme in WT-Chow vs. WT-DIO mice. (Two-way ANOVA, Šidák's multiple comparisons, n=6 for each group.). All error bars represent mean ± SEM. ns, not significant, *P < 0.05, **P < 0.01, ***P < 0.001, ****P < 0.0001.

Fig S2. Rapamycin does not regulate food intake or adiposity in *ob/ob* or *db/db* mice fed on HFD. OB-HFD: (**a**) Cumulative food intake (g), (**b**) Weight (%), (**c**) Fat mass (%) and (**d**) Lean mass (g) in *ob/ob* mice fed on HFD receiving 2 mg/kg/day rapamycin (RAP) plus 300 ng/hr leptin (LEP), RAP plus vehicle (VEH), VEH plus LEP, or VEH plus VEH (n = 10, 13, 11, 10 for each group; two-way ANOVA with Tukey's multiple comparisons for cumulative food intake and weight; two-way ANOVA with Šidák's multiple comparisons for fat mass and lean mass). DB-HFD: (**e**) Cumulative food intake (g), (**f**) Weight (%), (**g**) Fat mass (%) and (**h**) Lean mass (g) in *db/db* mice fed on HFD treated with RAP or VEH for 13 days (n = 4; two-way ANOVA, with Šidák's multiple comparisons). Body weight (g): (**i**) Body weight of WT-DIO mice treated with RAP vs. VEH for 14 days, and (**j**) RAP vs. VEH for 10 weeks (n = 9, 10, two-way ANOVA, with Šidák's multiple comparisons). (**k**) Body weight of WT-Chow mice treated with RAP plus 600 ng/hr leptin (LEP), RAP plus VEH, LEP plus VEH or VEH plus VEH (n = 12, 14, 14, 13 for each group, two-way ANOVA, with Tukey's multiple comparisons). (**l**) Body weight of OB-Chow mice treated with RAP plus 300 ng/hr leptin (LEP), RAP plus VEH, VEH plus LEP or VEH for 14 days (n = 5, 9, 7, 8 for each group, two-way ANOVA, with Tukey's multiple comparisons). (**m**) Body weight of DB-Chow mice treated with RAP vs. VEH for 14 days (n = 8, 5 for each group, two-way ANOVA, with Šidák's multiple comparisons). (**n**) Body weight of OB-HFD treated with RAP plus 300 ng/hr leptin (LEP), RAP plus VEH, VEH plus LEP or VEH plus VEH for 14 days (n = 10, 11, 13, 10 for each group, two-way ANOVA, with Tukey's multiple comparisons). (**o**) Body weight of DB-HFD mice treated with RAP vs. VEH for 13 days (n = 4, 4 for each group, two-way ANOVA, with Šidák's multiple comparisons). All error bars represent mean ± SEM. ns, not significant, *P < 0.05, **P < 0.01, ***P < 0.001, ****P < 0.0001.

Fig. S3. Rapamycin potentiates leptin in lean and aged mice. Low-dose LEP + RAP vs. High-dose LEP: (**a**) Cumulative food intake (g), (**b**) Weight (%), (**c**) Change in fat mass (%), (**d**) lean mass (g) in chow-fed lean mice treated with 600 ng/hr leptin (LEP600) or 150 ng/hr leptin (LEP150) for 14 days (Fat and lean mass measured at day 7; n=5 for each group, two-way ANOVA, with Šidák's multiple comparisons for comparisons of food intake, weight; two-tailed Student's t tests for fat mass and lean mass). (**e**) Cumulative food intake (g), (**f**) Weight (%), (**g**) Change in fat mass (%) and (**h**) lean mass (g) in chow-fed lean mice treated with 600 ng/hr leptin (LEP600) plus VEH or 150 ng/hr leptin (LEP150) plus RAP for 14 days. (n = 6 for each food-intake group, two-way ANOVA, with Šidák's multiple comparisons; n = 10, 3 for respective weight groups, two-way ANOVA, with Šidák's multiple comparisons; n = 4 for fat and lean mass, measured on day 7; two-tailed Student's t tests). Aged-Chow**:** (**i**) Cumulative food intake (g) and (**j**) Weight (%), (**k**) Change in body weight (g) of Aged-Chow mice (more than 16 months old) treated for 14 days with RAP plus LEP vs. VEH plus LEP (n=6, 7 for each group, two-way ANOVA, with Šidák's multiple comparisons) (**l**) Change in fat mass (%) and (**m**) Lean mass (g) in aged, chow-fed mice receiving RAP plus LEP vs. VEH plus LEP. (n=6, 7 for each group, two-way ANOVA, with Šidák's multiple comparisons for food intake, weight, and lean mass data; two-tailed Student's t-tests for Δ fat mass). Summary tables for (**n**) wildtype and (**o**) leptin-signaling-deficient mouse models. All error bars represent mean ± SEM. ns, not significant, *P < 0.05, **P < 0.01, ***P < 0.001, ****P < 0.0001.

Fig S4. Rapamycin regulates metabolism in addiction to decreasing food intake. (**a**) Body weight (%) in DIO mice treated with daily 2 mg/kg rapamycin (RAP) vs. vehicle (VEH). VEH group was pairfed to the RAP group for 5 weeks. (**b**) Body weight (g) in the same cohort (n = 6, 5 for each group, two-way ANOVA, with Šidák's multiple comparisons). (**c-f**) Metabolic parameters of DIO mice that received i.p. injections of 2 mg/kg RAP vs. VEH for 6 days, both groups were adlibitum fed (n = 8, 6 for each group, two-tailed Mann-Whitney tests). (**c**) Average RER (respiratory exchange ratio), (**d**) energy expenditure (kcal/g), (**e**) ambulatory activity (beam breaks/hr) and (**f**) daily food intake (n = 7, 6 for each group, two-tailed Mann-Whitney tests). All error bars represent mean ± SEM. ns, not significant, *P < 0.05, **P < 0.01, ***P < 0.001, ****P < 0.0001.

Fig S5. Whole-brain mTOR activity mapping and snRNA-seq analysis of differential gene expressions altered by rapamycin treatment in ob/ob mice. (**a**) Whole-brain mTOR activity (pS6) mapping in DIO vs. chow in the structure tree order and (**b**) in ranked descending order (n = 3, 3 for each group). (**c**) Schematic of experimental design for ob/ob mice that received 3-day daily i.p. injections of 2 mg/kg rapamycin vs. vehicle (n = 5589, 2345 nuclei profiled from the ARC for *ob/ob* mice treated with RAP vs. *ob/ob* mice treated with VEH). (**d**, **e**) Quantification of total numbers of regulated genes by RAP vs. VEH across unsupervised clusters and canonical cell types in *ob/ob* mice. (**f**, **g**) Volcano plots showing differentially expressed genes in cluster 12 (Pomc/Spag16+ cells) and total Pomc+ cells in response to RAP vs. VEH in *ob/ob* mice.

Fig S6. Melanocortin signaling is required for rapamycin-mediated leptin sensitization. (**a**) Body weight (g) in POMC-dTA and POMC-mCherry mice fed on chow receiving daily 2 mg/kg rapamycin (RAP) or vehicle (VEH) for 14 days (n = 10 for POMC-dTA+RAP, 12 for POMC-dTA+VEH, 8 for POMC-mCherry+RAP, 8 for POMC-mCherry+VEH, two-way ANOVA, with Tukey's multiple comparisons). (**b**) Body weight (g) in *mc4r-/-* fed on chow receiving RAP or VEH for 14 days. (n = 8, 10 for each group, two-way ANOVA, with Šidák's multiple comparisons). (**c**) Body weight (g) in *mc4r-/-* pairfed on HFD vs. DIO mice received RAP (n = 7, 6 for each group, two-way ANOVA, with Šidák's multiple comparisons). (**d**) Cumulative food intake (g), (**e**) Weight (%) and (**f**) GTT plasma glucose (mg/dL) in POMC-dTA mice fed on chow received 600 ng/hr leptin (LEP) vs. VEH for 7 days (n = 7, 7 for each group, two-way ANOVA, with Šidák's multiple comparisons). GTT was conducted at Day 7, 2 mg/kg/lean mass dosage was used for glucose injections. (**g**) Cumulative food intake (g), (**h**) Weight (%) and (**i**) GTT plasma glucose (mg/dL) in POMC-dTA mice fed chow received 150 ng/hr leptin (LEP) plus RAP or RAP plus VEH for 7 days (n = 7, 7 for each group, two-way ANOVA, with Šidák's multiple comparisons). GTT was conducted at Day 6. (**j**) Cumulative food intake (g), (**k**) Weight (%) and (**l**) GTT plasma glucose (mg/dL) in *mc4r-/-* mice fed on chow received 150 ng/hr leptin (LEP) vs. VEH for 14 days (n = 4, 4 for each group, two-way ANOVA, with Šidák's multiple comparisons). GTT was conducted at Day 7. (**m**) Cumulative food intake (g), (**n**) Weight (%) and (**o**) GTT plasma glucose (mg/dL) in *mc4r-/-* mice fed on chow received 150 ng/hr leptin (LEP) plus RAP vs. VEH plus RAP for 14 days (n = 9, 10 for each group, two-way ANOVA, with Šidák's multiple comparisons). GTT was conducted at Day 7. (**p**) Change in fat mass (%) and (**q**) lean mass (g) after 14-day treatment of 150 ng/hr leptin (LEP plus RAP in *mc4r-/-* vs. WT on chow. n = 9, 10 for each group, two-tailed Mann-Whitney tests). All error bars represent mean ± SEM. ns, not significant, *P < 0.05, **P < 0.01, ***P < 0.001, ****P < 0.0001.

Fig S7. Summary tables for rapamycin and leptin responses in melanocortin-signaling-deficient mouse models. (**a**) POMC-dTA vs. POMC-mCherry mice, (**b**) Ad libitum chow fed *mc4r-/-* vs. WT mice (**c**) Pair-fat *mc4r-/-* mice on HFD vs. WT-DIO. The responses were summarized based on data from Fig. 5 and Fig. S6.

Fig S8. POMC-specific mTOR activation causes leptin resistance in chow-fed mice and even in *ob/ob* mice, which cannot be reversed by rapamycin in the absence of leptin. (**a**) Daily food intake at 20th week of age (g) and (**b**) Body weight (g) over 20 weeks, (**c**) Fat mass (%) and (**d**) Lean mass (g) of POMC$^{tsc1-/-}$ versus wild-type littermate controls at 20th week of age (n = 10, 13; two-way ANOVA, with Šidák's multiple comparisons for Body weight; two-tailed Student's t-tests for Food intake, Fat mass and Lean mass comparisons). (**e**) Daily food intake (g) and (**f**) Body weight (g) over 20 weeks in AgRP$^{tsc1-/-}$, *Cre- tsc1 fl/fl*, AgRP-Cre+, AgRP-Cre-. (**g**) Fat mass and (**h**) lean mass of AgRP$^{tsc1-/-}$, *Cre- tsc1 fl/fl*, AgRP-Cre+, AgRP-Cre- at 20th week of age (n = 13, 11, 9, 6 for each group, two-tailed Student's t-tests for Food intake; two-way ANOVA, with Tukey's multiple comparisons for body weight; one-way ANOVA, with Dunnett's multiple comparisons for fat mass and lean mass). (**i**) Body weight (g) during 4 weeks of 150 ng/hr Leptin (LEP) or vehicle (VEH) treatment in *ob/ob* POMC$^{tsc1-/-}$ (OB- POMC$^{tsc1-/-}$), *ob/ob* POMC$^{tsc1+/-}$ and *ob/ob* POMC$^{tsc1+/+}$ (n = 19, 6, 20 for each group). (**j**) Body weight (g) during 4 weeks of 150 ng/hr leptin (LEP) plus daily 2 mg/kg rapamycin (RAP) vs. VEH plus RAP treatment in OB-POMC$^{tsc1-/-}$ and OB-controls (n = 6 for +OB-POMC$^{tsc1-/-}$ +RAP+LEP, n = 9 for OB-controls +RAP+LEP, n = 3 for OB- POMC$^{tsc1-/-}$ +RAP+VEH, n = 8 for OB-controls +RAP+VEH). All error bars represent mean ± SEM. ns, not significant, *P < 0.05, **P < 0.01, ***P < 0.001, ****P < 0.0001.

Fig S9. Representative histograms of POMC firing rates. (**a**) Firing rate histograms for individual cells during bath application of leptin (100nM, 20 minutes) from POMC neurons of chow fed, DIO, DIO receiving vehicle injections (3 days) and DIO mice receiving rapamycin (3 days)(from top to bottom). (**b**) Firing rate (Hz) is calculated in 10s bins. Leptin 100nM is bath applied for 20 minutes (blue box). Calibration bar for the DIO mice is 1Hz while for all other traces it is 2Hz and 5 mins.

Fig S10. CRISPR-guided POMC-specific knockouts of *Wdr24* and *Rheb* mitigates weight gain of mice fed on HFD. (**a**) Diagram illustrates the RHEB and GATRO2/WDR24 in the mTOR pathway. (**b**) Schematic depicts experimental design of AAV-delivery to ARC of POMC-Cas9 mice. (**c**) Cumulative food intake (g) and (**d**) Change in weight (g) during 3 weeks on chow diet. (**e**) Cumulative food intake (g) and (**f**) Change in weight (g) during 3 weeks on HFD. (n = 8, 6, 5 for the cumulative food intake on chow or HFD of the control, Wdr24, Rheb group, respectively; n = 8, 13, 12 for the weight on chow or HFD of the control, Wdr24, Rheb group, respectively. Two-way ANOVA, with Dunnett's multiple comparisons). All error bars represent mean ± SEM. ns, not significant, *P < 0.05, **P < 0.01, ***P < 0.001, ****P < 0.0001.

Figure1

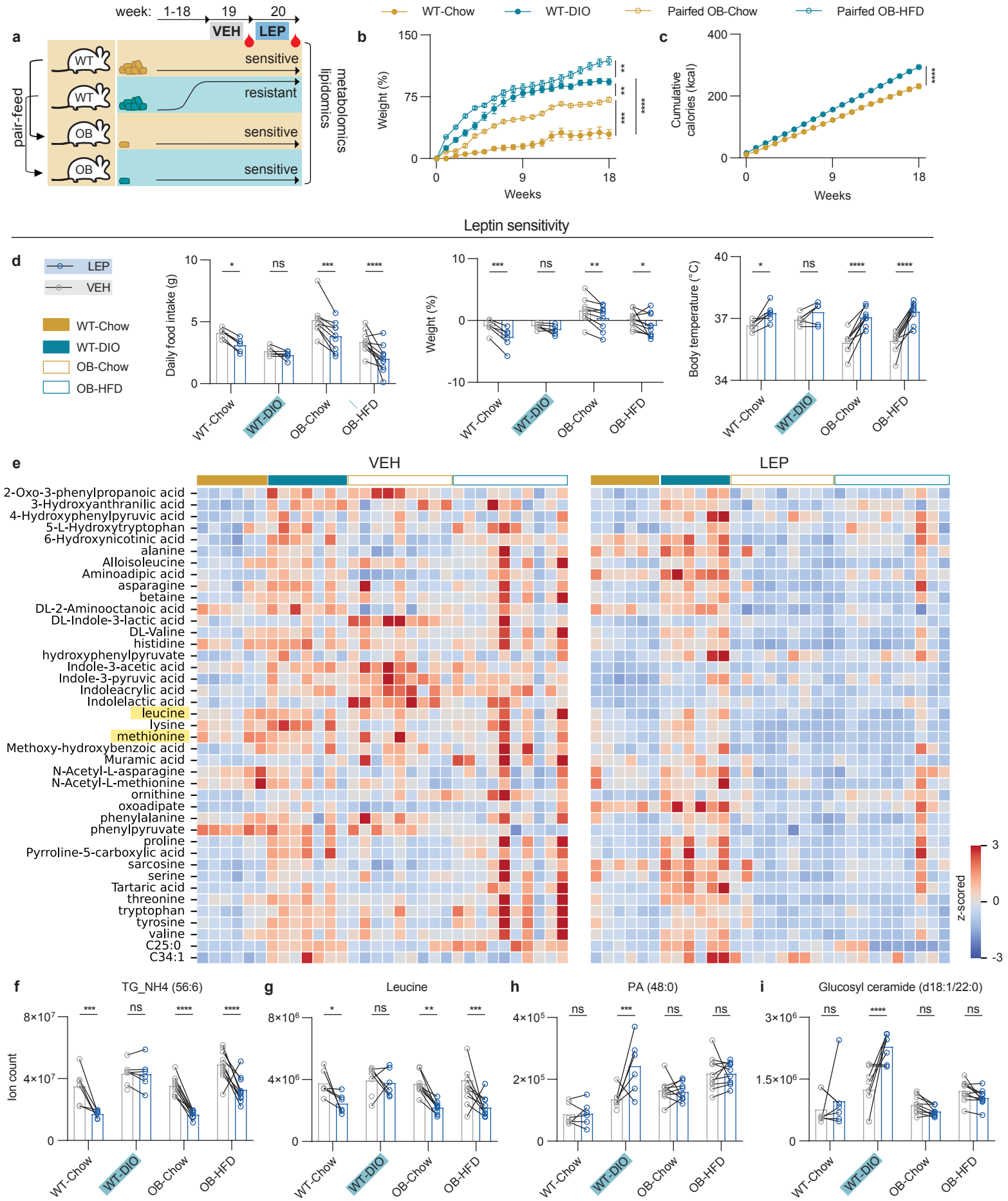
week: 1-18 19 20
VEH
LEP
a
pair-feed
WT
WT
OB
OB
sensitive
resistant
sensitive
sensitive
metabolomics
lipidomics
b
WT-Chow
WT-DIO
Pairfed OB-Chow
Pairfed OB-HFD
Weight (%)
Weeks
c
Cumulative calories (kcal)
Weeks
Leptin sensitivity
d
LEP
VEH
WT-Chow
WT-DIO
OB-Chow
OB-HFD
Daily food intake (g)
Weight (%)
Body temperature (°C)
e
VEH
LEP
2-Oxo-3-phenylpropanoic acid
3-Hydroxyanthranilic acid
4-Hydroxyphenylpyruvic acid
5-L-Hydroxytryptophan
6-Hydroxynicotinic acid
alanine
Alloisoleucine
Aminoadipic acid
asparagine
betaine
DL-2-Aminooctanoic acid
DL-Indole-3-lactic acid
DL-Valine
histidine
hydroxyphenylpyruvate
Indole-3-acetic acid
Indole-3-pyruvic acid
Indoleacrylic acid
Indolelactic acid
leucine
lysine
methionine
Methoxy-hydroxybenzoic acid
Muramic acid
N-Acetyl-L-asparagine
N-Acetyl-L-methionine
ornithine
oxoadipate
phenylalanine
phenylpyruvate
proline
Pyrroline-5-carboxylic acid
sarcosine
serine
Tartaric acid
threonine
tryptophan
tyrosine
valine
C25:0
C34:1
z-scored
f
TG_NH4 (56:6)
Ion count
g
Leucine
h
PA (48:0)
i
Glucosyl ceramide (d18:1/22:0)

Figure 2

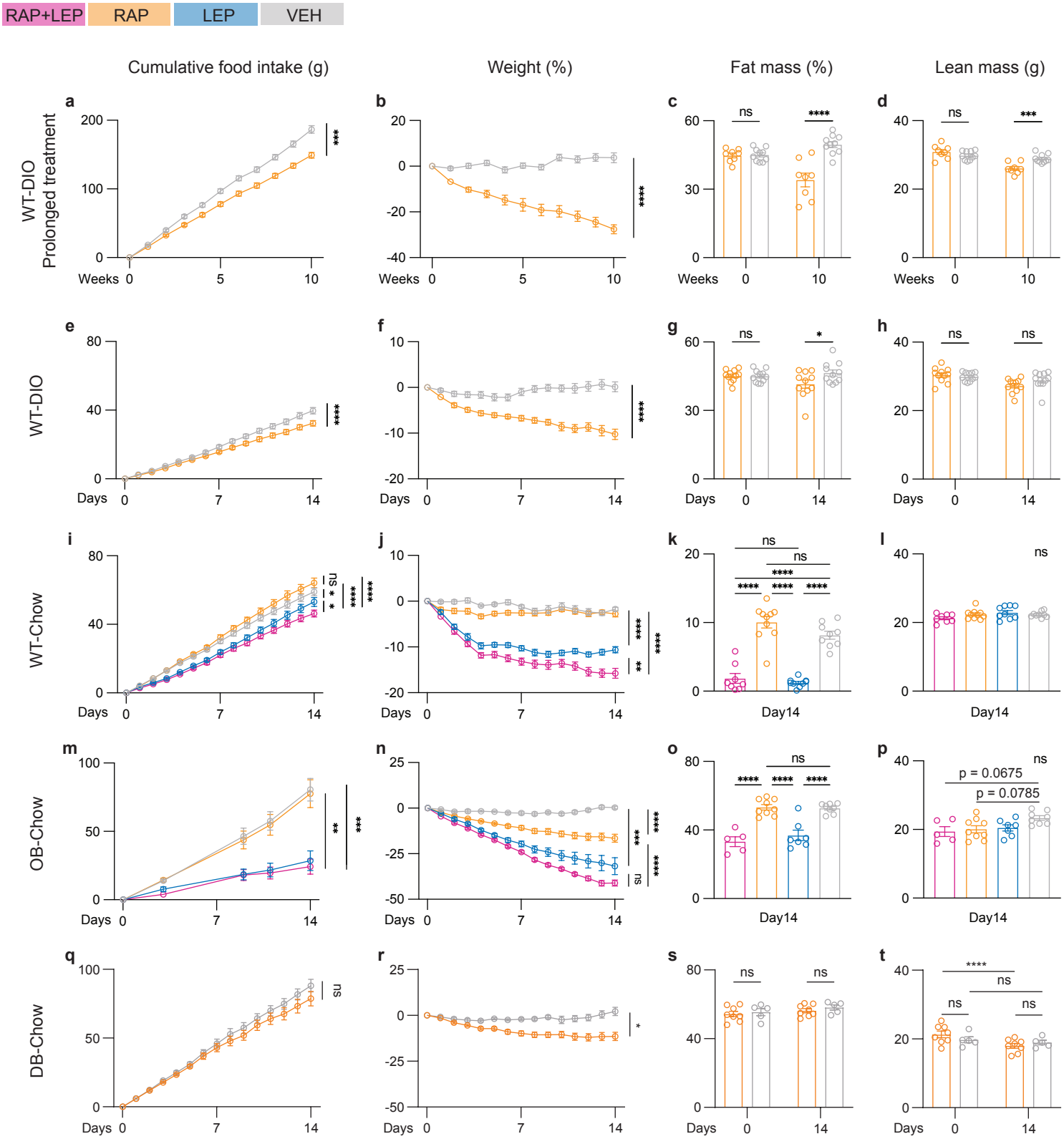
RAP+LEP
RAP
LEP
VEH
Cumulative food intake (g)
Weight (%)
Fat mass (%)
Lean mass (g)
WT-DIO Prolonged treatment
WT-DIO
WT-Chow
OB-Chow
DB-Chow
Weeks
Days
Day14
ns
p = 0.0675
p = 0.0785

Figure 3

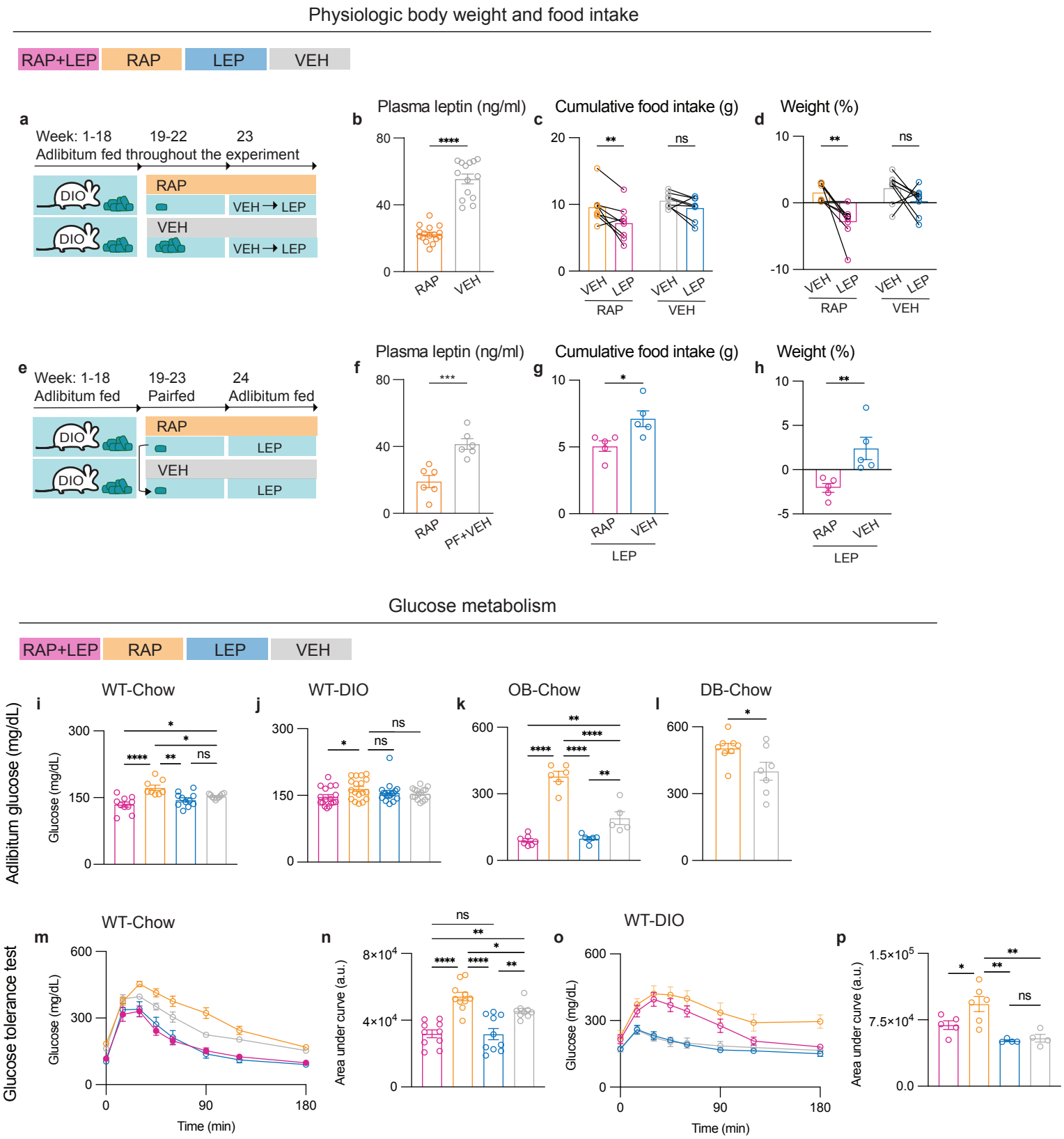
Physiologic body weight and food intake
RAP+LEP
RAP
LEP
VEH
a
Week: 1-18
19-22
23
Adlibitum fed throughout the experiment
DIO
RAP
VEH → LEP
VEH
b
Plasma leptin (ng/ml)
c
Cumulative food intake (g)
d
Weight (%)
e
Week: 1-18
Adlibitum fed
19-23
Pairfed
24
Adlibitum fed
LEP
f
g
h
PF+VEH
Glucose metabolism
Adlibitum glucose (mg/dL)
i
WT-Chow
j
WT-DIO
k
OB-Chow
l
DB-Chow
Glucose (mg/dL)
Glucose tolerance test
m
n
o
p
Area under curve (a.u.)
Time (min)

Figure 4

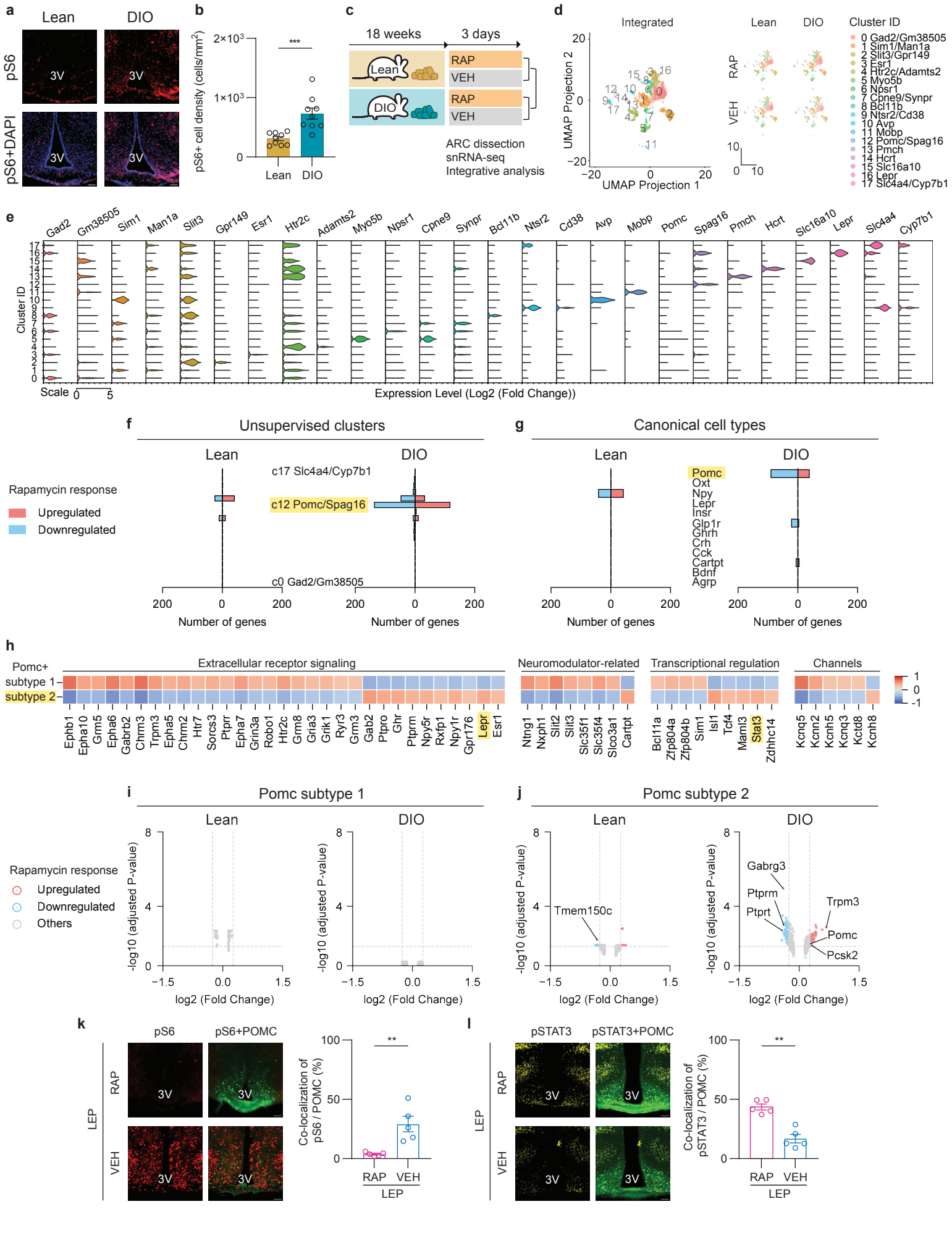
a
Lean
DIO
pS6
pS6+DAPI
3V
b
pS6+ cell density (cells/mm²)
2×10³
1×10³
0
***
Lean
DIO
c
18 weeks
3 days
Lean
DIO
RAP
VEH
RAP
VEH
ARC dissection
snRNA-seq
Integrative analysis
d
Integrated
UMAP Projection 2
UMAP Projection 1
Lean
DIO
RAP
VEH
Cluster ID
0 Gad2/Gm38505
1 Sim1/Man1a
2 Slit3/Gpr149
3 Esr1
4 Htr2c/Adamts2
5 Myo5b
6 Npsr1
7 Cpne9/Synpr
8 Bcl11b
9 Ntsr2/Cd38
10 Avp
11 Mobp
12 Pomc/Spag16
13 Pmch
14 Hcrt
15 Slc16a10
16 Lepr
17 Slc4a4/Cyp7b1
e
Gad2
Gm38505
Sim1
Man1a
Slit3
Gpr149
Esr1
Htr2c
Adamts2
Myo5b
Npsr1
Cpne9
Synpr
Bcl11b
Ntsr2
Cd38
Avp
Mobp
Pomc
Spag16
Pmch
Hcrt
Slc16a10
Lepr
Slc4a4
Cyp7b1
Cluster ID
Scale
Expression Level (Log2 (Fold Change))
f
Unsupervised clusters
Lean
DIO
c17 Slc4a4/Cyp7b1
c12 Pomc/Spag16
c0 Gad2/Gm38505
Rapamycin response
Upregulated
Downregulated
Number of genes
g
Canonical cell types
Lean
DIO
Pomc
Oxt
Npy
Lepr
Insr
Glp1r
Ghrh
Crh
Cck
Cartpt
Bdnf
Agrp
Number of genes
h
Pomc+
subtype 1
subtype 2
Extracellular receptor signaling
Neuromodulator-related
Transcriptional regulation
Channels
Ephb1
Epha10
Grm5
Epha6
Gabrb2
Chrm3
Trpm3
Epha5
Chrm2
Htr7
Sorcs3
Ptpr
Epha7
Grin3a
Robo1
Htr2c
Grm8
Gria3
Grik1
Ryr3
Grm3
Gab2
Ptpro
Ghr
Ptprm
Npy5r
Rxfp1
Npy1r
Gpr176
Lepr
Esr1
Ntng1
Nxph1
Slit2
Slit3
Slc35f1
Slc35f4
Slco3a1
Cartpt
Bcl11a
Zfp804a
Zfp804b
Sim1
Isl1
Tcf4
Maml3
Stat3
Zdhhc14
Kcnq5
Kcnn2
Kcnh5
Kcnq3
Kcnd8
Kcnh8
i
Pomc subtype 1
Lean
DIO
Rapamycin response
Upregulated
Downregulated
Others
-log10 (adjusted P-value)
log2 (Fold Change)
j
Pomc subtype 2
Lean
DIO
Tmem150c
Gabrg3
Ptprm
Ptprt
Trpm3
Pomc
Pcsk2
k
pS6
pS6+POMC
LEP
RAP
VEH
Co-localization of pS6 / POMC (%)
**
l
pSTAT3
pSTAT3+POMC
Co-localization of pSTAT3 / POMC (%)
**

Figure 5

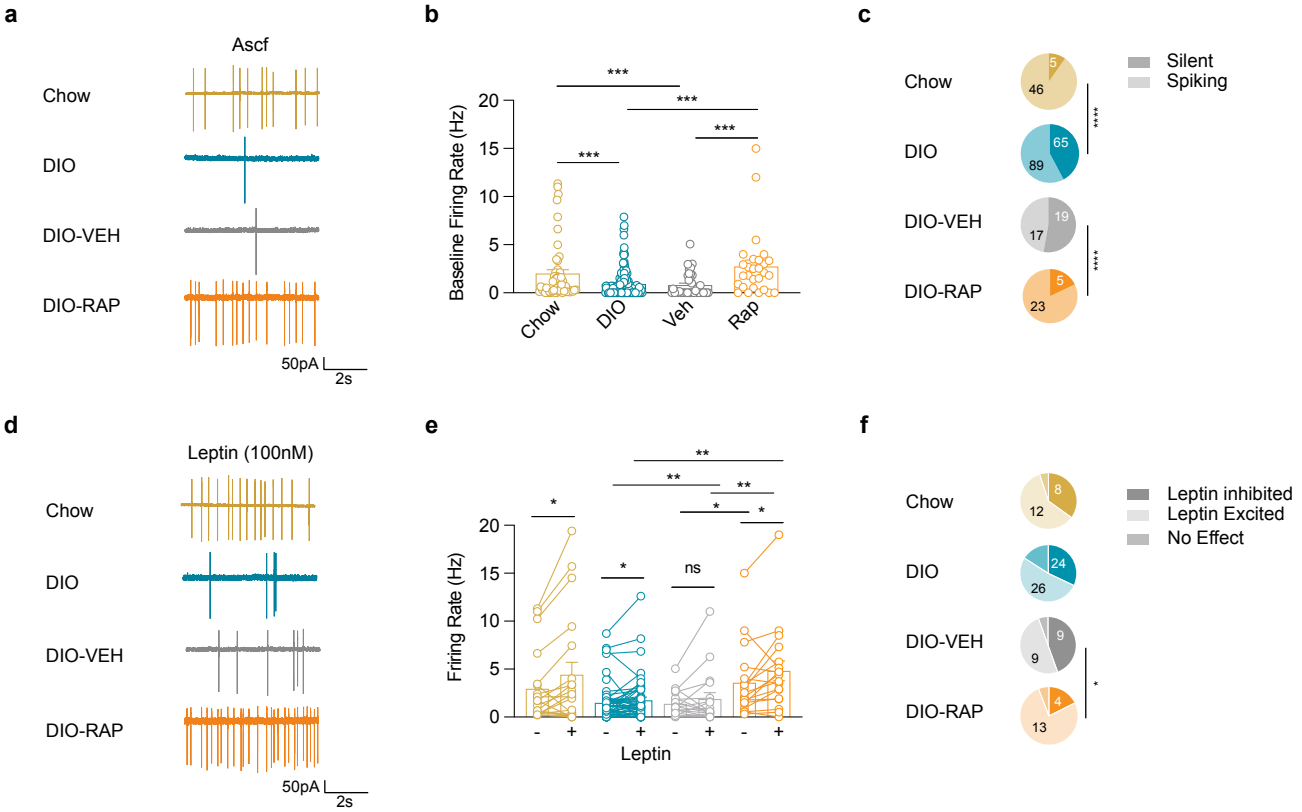
a
Ascf
Chow
DIO
DIO-VEH
DIO-RAP
50pA
2s
b
Baseline Firing Rate (Hz)
20
15
10
5
0
***
***
***
***
Chow
DIO
Veh
Rap
c
Chow
DIO
DIO-VEH
DIO-RAP
5
46
65
89
19
17
5
23
****
****
Silent
Spiking
d
Leptin (100nM)
Chow
DIO
DIO-VEH
DIO-RAP
50pA
2s
e
Firiring Rate (Hz)
20
15
10
5
0
*
*
ns
**
**
**
*
*
- + - + - + - +
Leptin
f
Chow
DIO
DIO-VEH
DIO-RAP
8
12
24
26
9
9
4
13
*
Leptin inhibited
Leptin Excited
No Effect

Figure 6

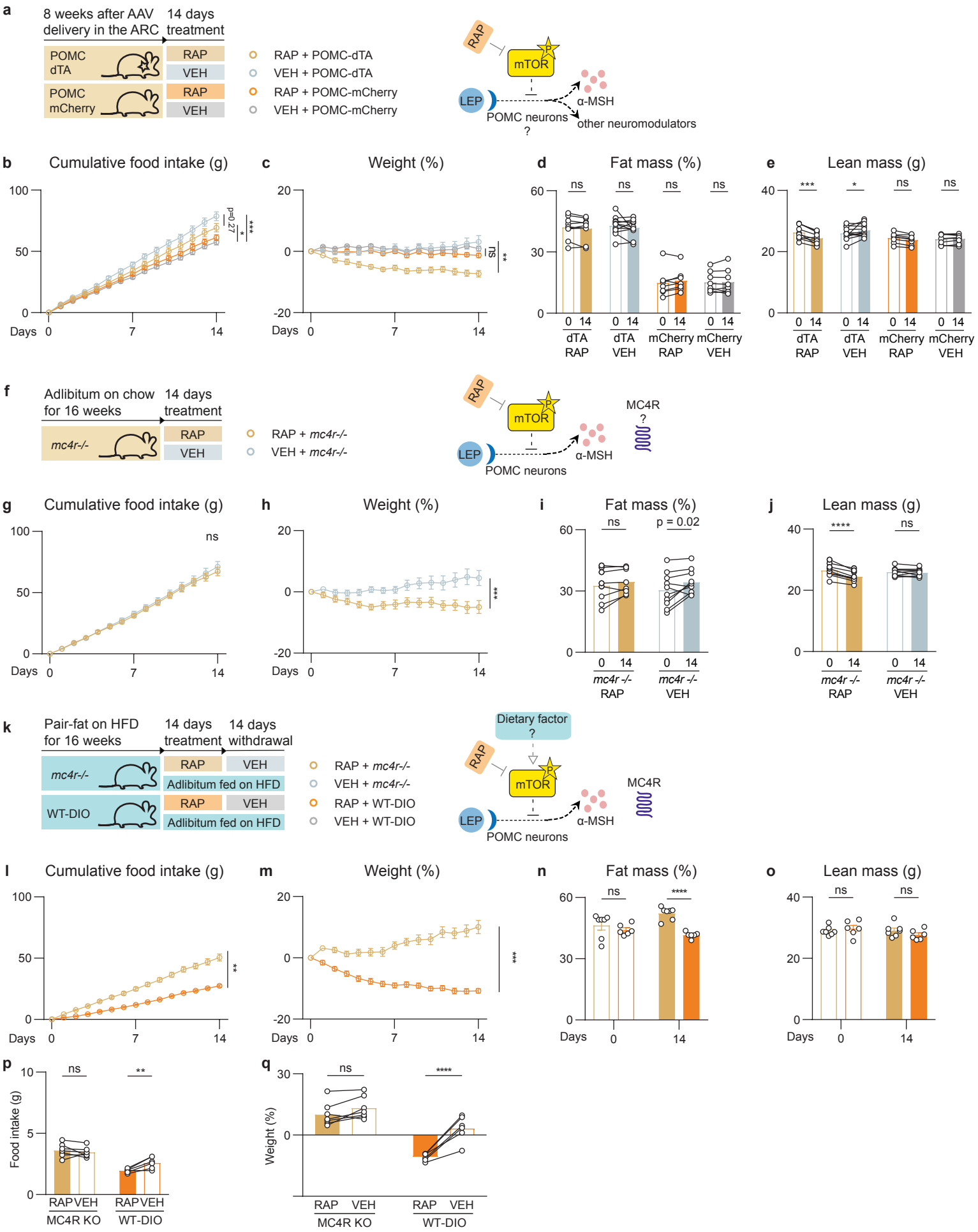
a
8 weeks after AAV delivery in the ARC
14 days treatment
POMC dTA
RAP
VEH
POMC mCherry
RAP
VEH
RAP + POMC-dTA
VEH + POMC-dTA
RAP + POMC-mCherry
VEH + POMC-mCherry
RAP
mTOR
P
LEP
POMC neurons
?
α-MSH
other neuromodulators
b
Cumulative food intake (g)
Days
p=0.27
*
***
c
Weight (%)
ns
**
d
Fat mass (%)
ns
dTA RAP
dTA VEH
mCherry RAP
mCherry VEH
e
Lean mass (g)
***
*
f
Adlibitum on chow for 16 weeks
14 days treatment
mc4r-/-
RAP
VEH
RAP + mc4r-/-
VEH + mc4r-/-
MC4R
?
g
Cumulative food intake (g)
h
Weight (%)
i
Fat mass (%)
p = 0.02
j
Lean mass (g)
****
mc4r -/- RAP
mc4r -/- VEH
k
Pair-fat on HFD for 16 weeks
14 days treatment
14 days withdrawal
mc4r-/-
RAP
VEH
Adlibitum fed on HFD
WT-DIO
RAP + WT-DIO
VEH + WT-DIO
Dietary factor
?
l
Cumulative food intake (g)
m
Weight (%)
n
Fat mass (%)
o
Lean mass (g)
p
Food intake (g)
MC4R KO
WT-DIO
q
Weight (%)

Figure 7

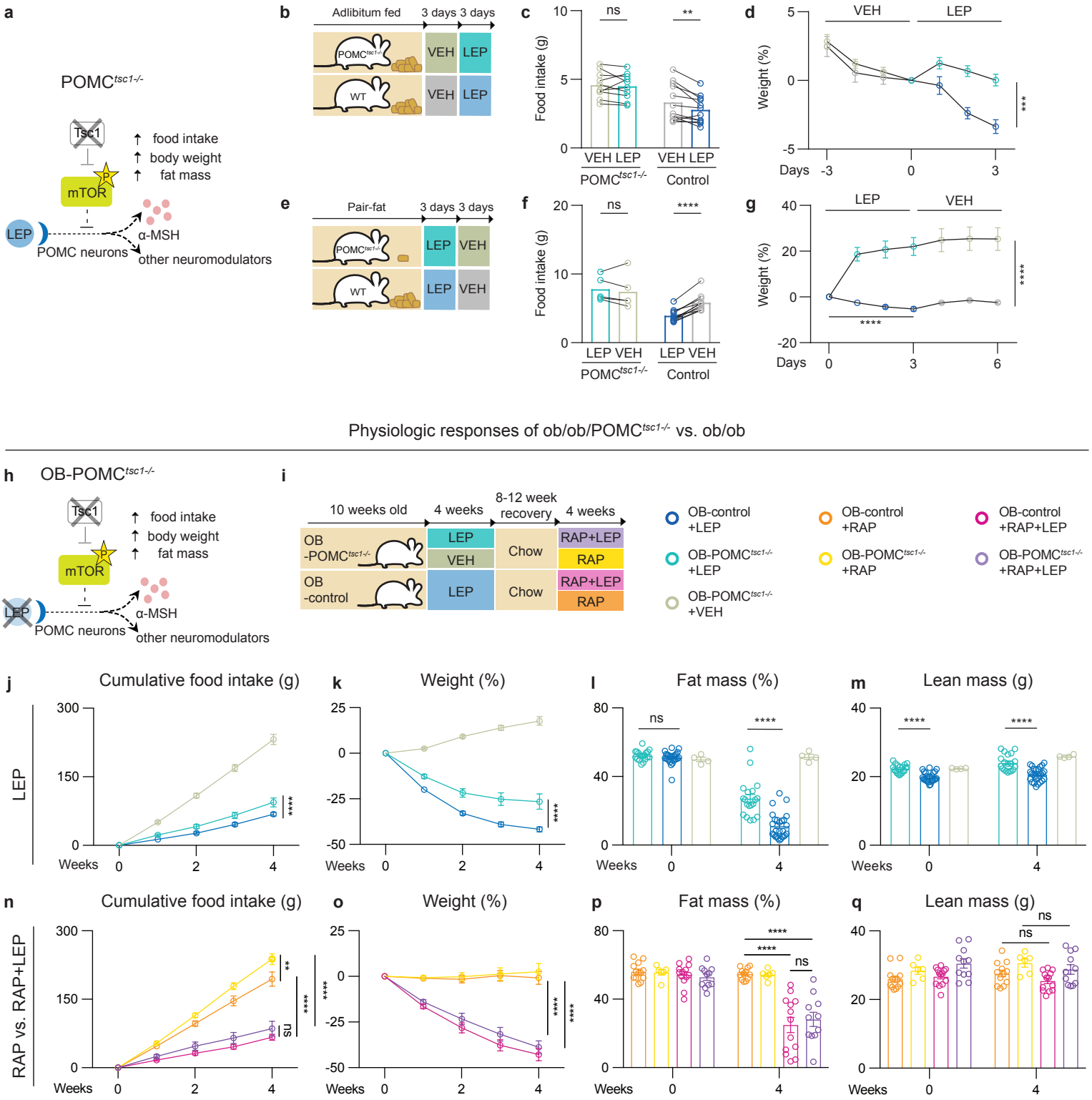
a
POMC tsc1-/-
Tsc1
mTOR
P
↑ food intake
↑ body weight
↑ fat mass
LEP
α-MSH
POMC neurons
other neuromodulators
b
Adlibitum fed
3 days 3 days
POMC tsc1-/-
WT
VEH
LEP
c
ns
**
Food intake (g)
VEH LEP
POMC tsc1-/-
Control
d
VEH
LEP
Weight (%)
***
Days
e
Pair-fat
3 days 3 days
f
****
g
Physiologic responses of ob/ob/POMC tsc1-/- vs. ob/ob
h
OB-POMC tsc1-/-
i
10 weeks old
4 weeks
8-12 week recovery
4 weeks
OB -POMC tsc1-/-
OB -control
Chow
RAP+LEP
RAP
OB-control +LEP
OB-POMC tsc1-/- +LEP
OB-POMC tsc1-/- +VEH
OB-control +RAP
OB-POMC tsc1-/- +RAP
OB-control +RAP+LEP
OB-POMC tsc1-/- +RAP+LEP
j
Cumulative food intake (g)
LEP
Weeks
k
Weight (%)
l
Fat mass (%)
m
Lean mass (g)
n
Cumulative food intake (g)
RAP vs. RAP+LEP
o
Weight (%)
p
Fat mass (%)
q
Lean mass (g)

Figure S1

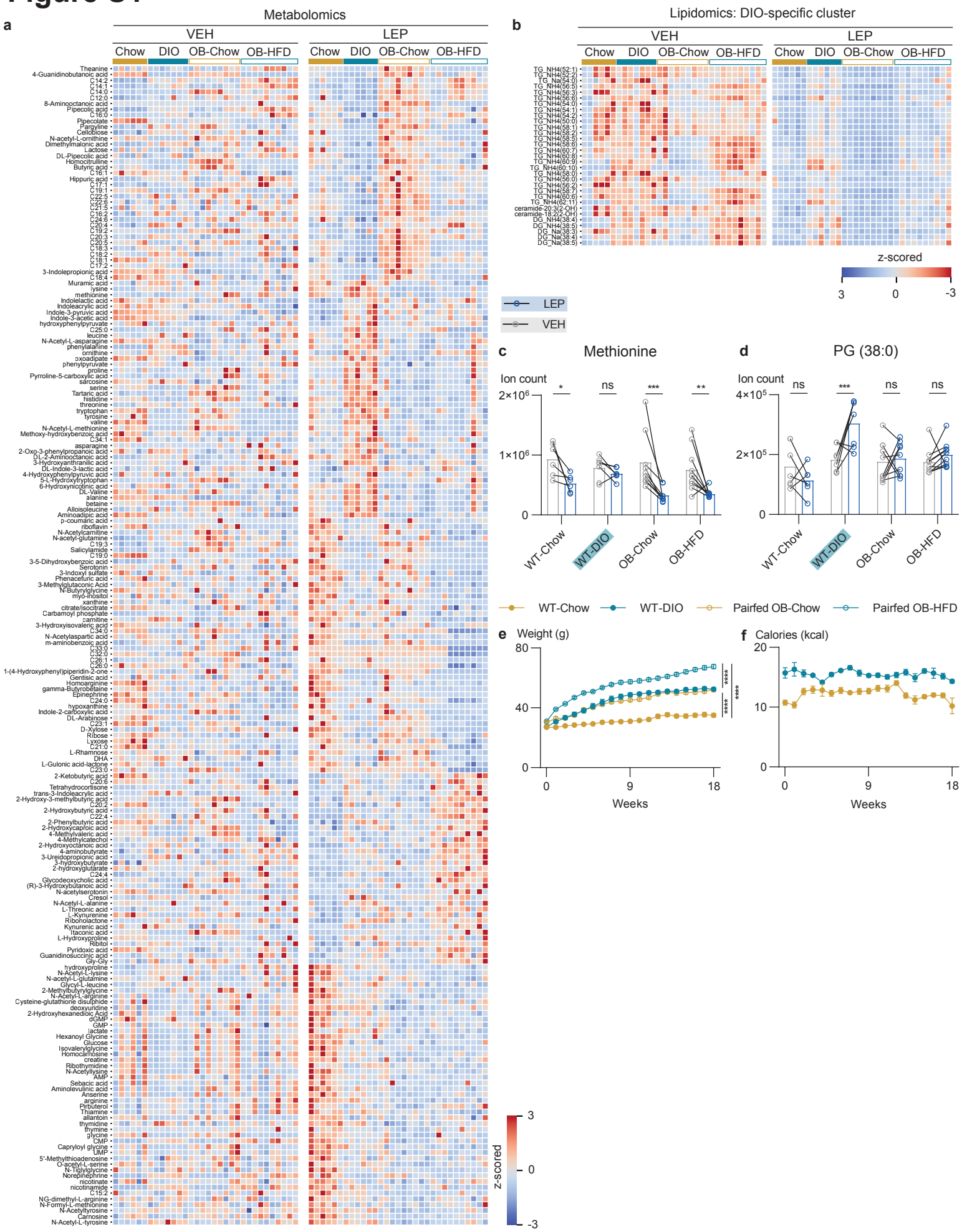
a
Metabolomics
VEH
LEP
Chow
DIO
OB-Chow
OB-HFD
b
Lipidomics: DIO-specific cluster
z-scored
3
0
-3
LEP
VEH
c
Methionine
Ion count
2×10^6
1×10^6
0
ns
***
**
WT-Chow
WT-DIO
OB-Chow
OB-HFD
d
PG (38:0)
4×10^5
2×10^5
WT-Chow
WT-DIO
Pairfed OB-Chow
Pairfed OB-HFD
e
Weight (g)
80
40
0
9
18
Weeks
f
Calories (kcal)
20
10

Figure S2

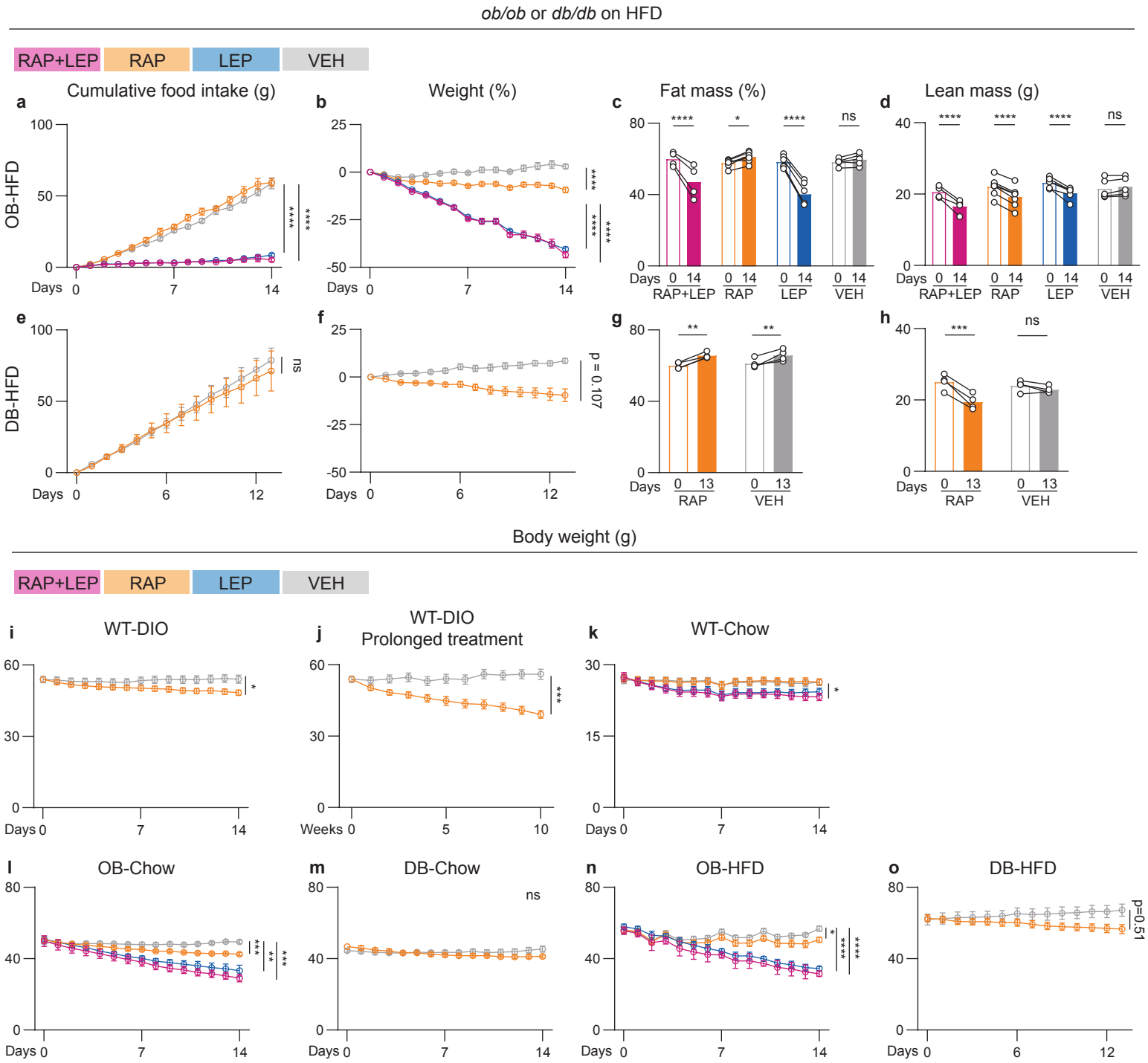
ob/ob or db/db on HFD
RAP+LEP
RAP
LEP
VEH
a
Cumulative food intake (g)
OB-HFD
Days
b
Weight (%)
c
Fat mass (%)
d
Lean mass (g)
e
DB-HFD
f
p = 0.107
g
h
Body weight (g)
i
WT-DIO
j
WT-DIO
Prolonged treatment
Weeks
k
WT-Chow
l
OB-Chow
m
DB-Chow
n
OB-HFD
o
DB-HFD
p=0.51

Figure S3

Physiologic responses of low-dose leptin plus rapamycin vs. high-dose leptin

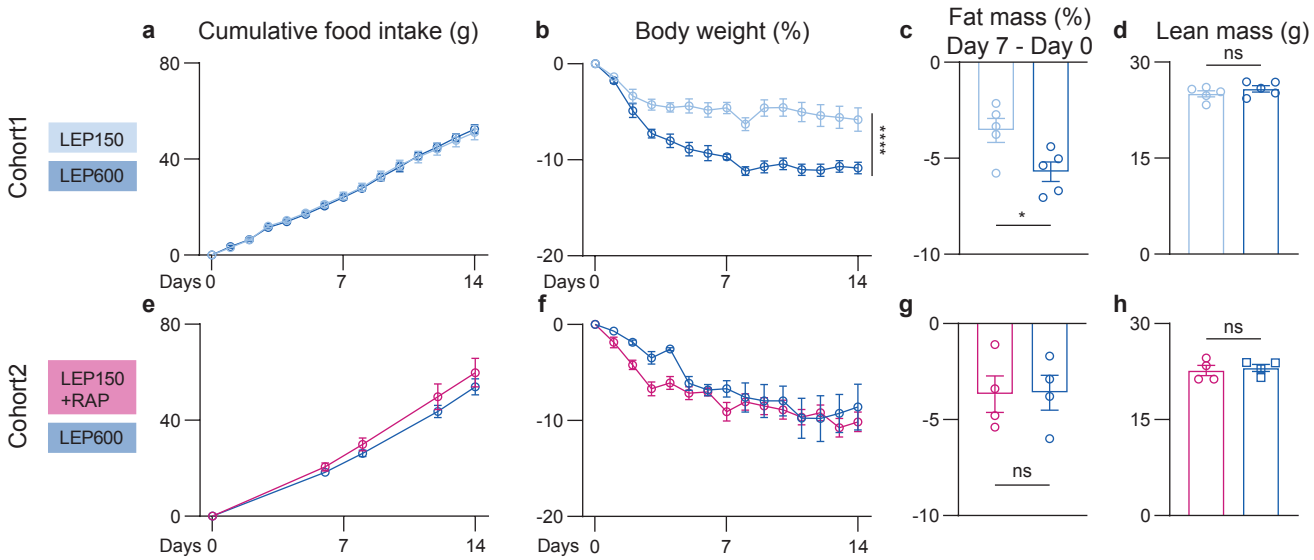

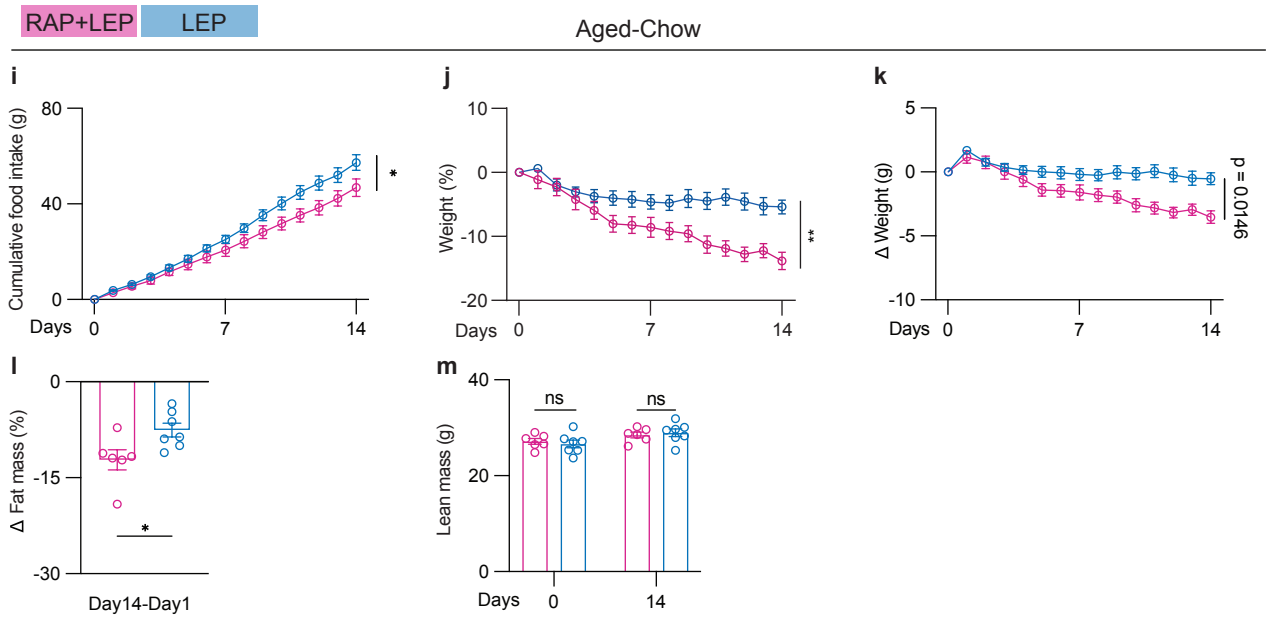

Summary tables for mouse models

n

Wild-type mouse models		14 days treatment	Food Intake	Weight	% Fat	Lean mass
WT-DIO	Obese	RAP	↓	↓	↓	–
		VEH	–	–	–	–
WT-Chow	Lean	RAP+LEP	↓	↓	↓	–
		RAP	–	–	–	–
		LEP	↓	↓	↓	–
		VEH	–	–	–	–
WT-Chow	Lean	LEP 150	–	–	–	–
		LEP 600	↓	↓	↓	–
		LEP 150+RAP	↓	↓	↓	–
WT-aged	Mildly obese	RAP+LEP	↓	↓	↓	–
		LEP	–	–	–	–

o

Leptin-signaling-deficient mouse models		14 days treatment	Food Intake	Weight	% Fat	Lean mass
OB-Chow	Obese	RAP+LEP	↓	↓	↓	–
		RAP	–	↓	–	–
		LEP	↓	↓	↓	–
		VEH	–	–	–	–
OB-HFD	Obese	RAP+LEP	↓	↓	↓	↓
		RAP	–	↓	↑	↓
		LEP	↓	↓	↓	↓
		VEH	–	–	–	–
DB-Chow	Obese	RAP	–	–	–	↓
		VEH	–	–	–	–
DB-HFD	Obese	RAP	–	↓	↑	↓
		VEH	–	↑	↑	–

Figure S4

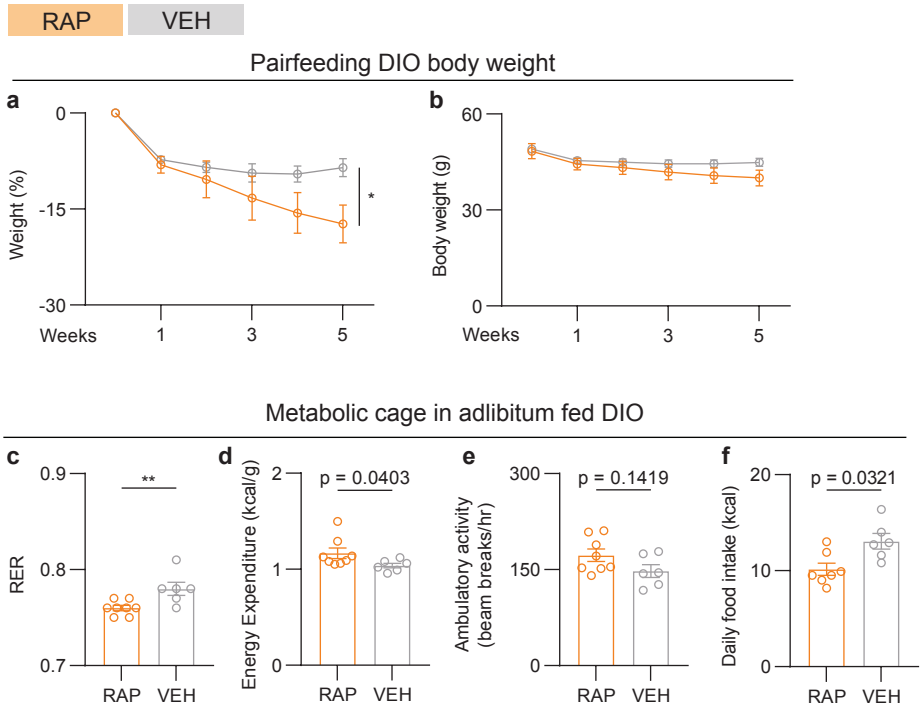
RAP
VEH
Pairfeeding DIO body weight
a
Weight (%)
0
-15
-30
Weeks
1
3
5
*
b
Body weight (g)
60
30
0
Weeks
1
3
5
Metabolic cage in adlibitum fed DIO
c
RER
0.9
0.8
0.7
**
RAP
VEH
d
Energy Expenditure (kcal/g)
2
1
0
p = 0.0403
RAP
VEH
e
Ambulatory activity (beam breaks/hr)
300
150
0
p = 0.1419
RAP
VEH
f
Daily food intake (kcal)
20
10
0
p = 0.0321
RAP
VEH

Figure S5

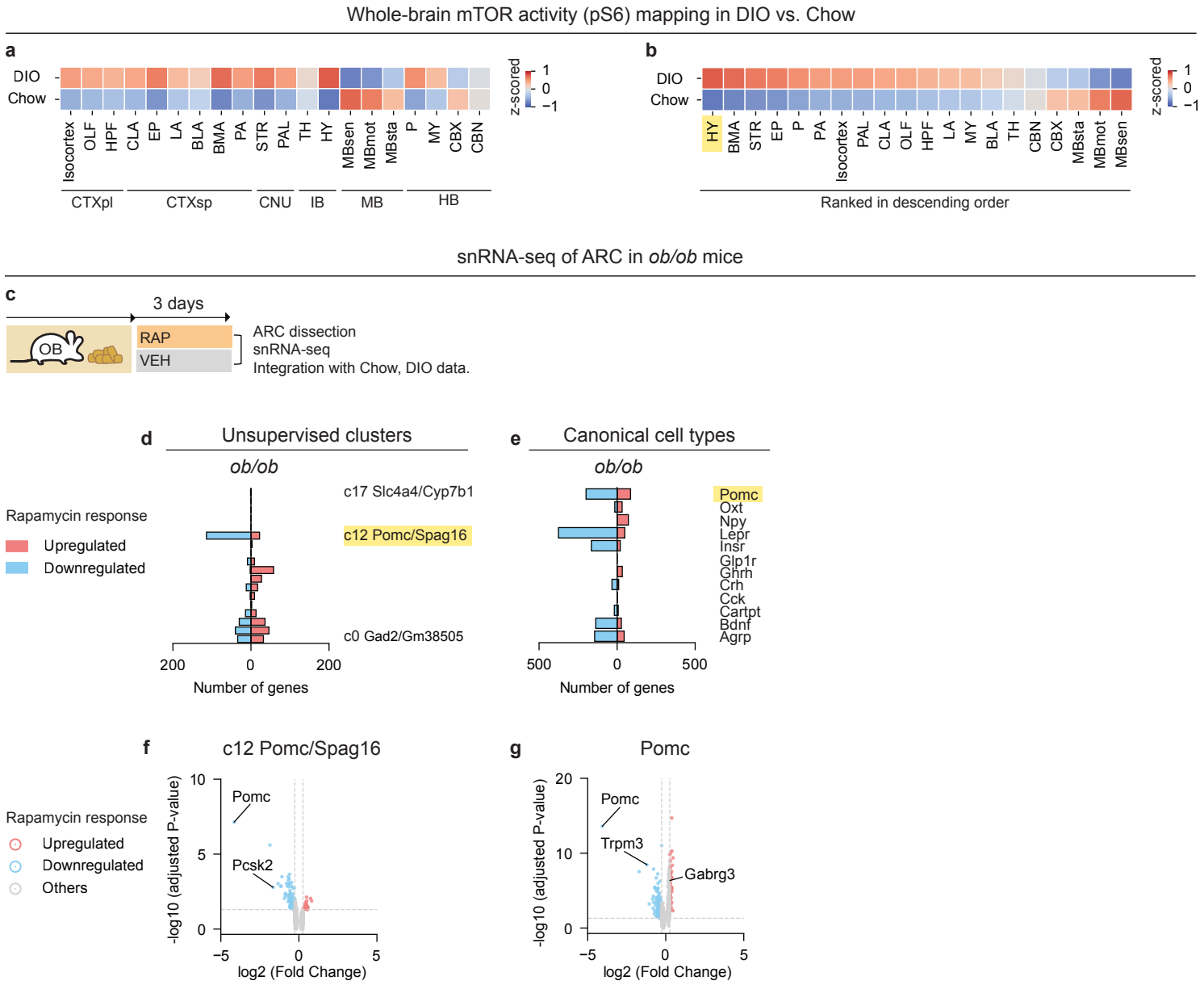
Whole-brain mTOR activity (pS6) mapping in DIO vs. Chow
a
DIO
Chow
Isocortex
OLF
HPF
CLA
EP
LA
BLA
BMA
PA
STR
PAL
TH
HY
MBsen
MBmot
MBsta
P
MY
CBX
CBN
CTXpl
CTXsp
CNU
IB
MB
HB
z-scored
1
0
−1
b
DIO
Chow
HY
BMA
STR
EP
P
PA
Isocortex
PAL
CLA
OLF
HPF
LA
MY
BLA
TH
CBN
CBX
MBsta
MBmot
MBsen
Ranked in descending order
z-scored
1
0
−1
snRNA-seq of ARC in ob/ob mice
c
3 days
OB
RAP
VEH
ARC dissection
snRNA-seq
Integration with Chow, DIO data.
d
Unsupervised clusters
ob/ob
Rapamycin response
Upregulated
Downregulated
c17 Slc4a4/Cyp7b1
c12 Pomc/Spag16
c0 Gad2/Gm38505
200
0
200
Number of genes
e
Canonical cell types
ob/ob
Pomc
Oxt
Npy
Lepr
Insr
Glp1r
Ghrh
Crh
Cck
Cartpt
Bdnf
Agrp
500
0
500
Number of genes
f
c12 Pomc/Spag16
Rapamycin response
Upregulated
Downregulated
Others
Pomc
Pcsk2
-log10 (adjusted P-value)
10
5
0
−5
0
5
log2 (Fold Change)
g
Pomc
Pomc
Trpm3
Gabrg3
-log10 (adjusted P-value)
20
10
0
−5
0
5
log2 (Fold Change)

Figure S6

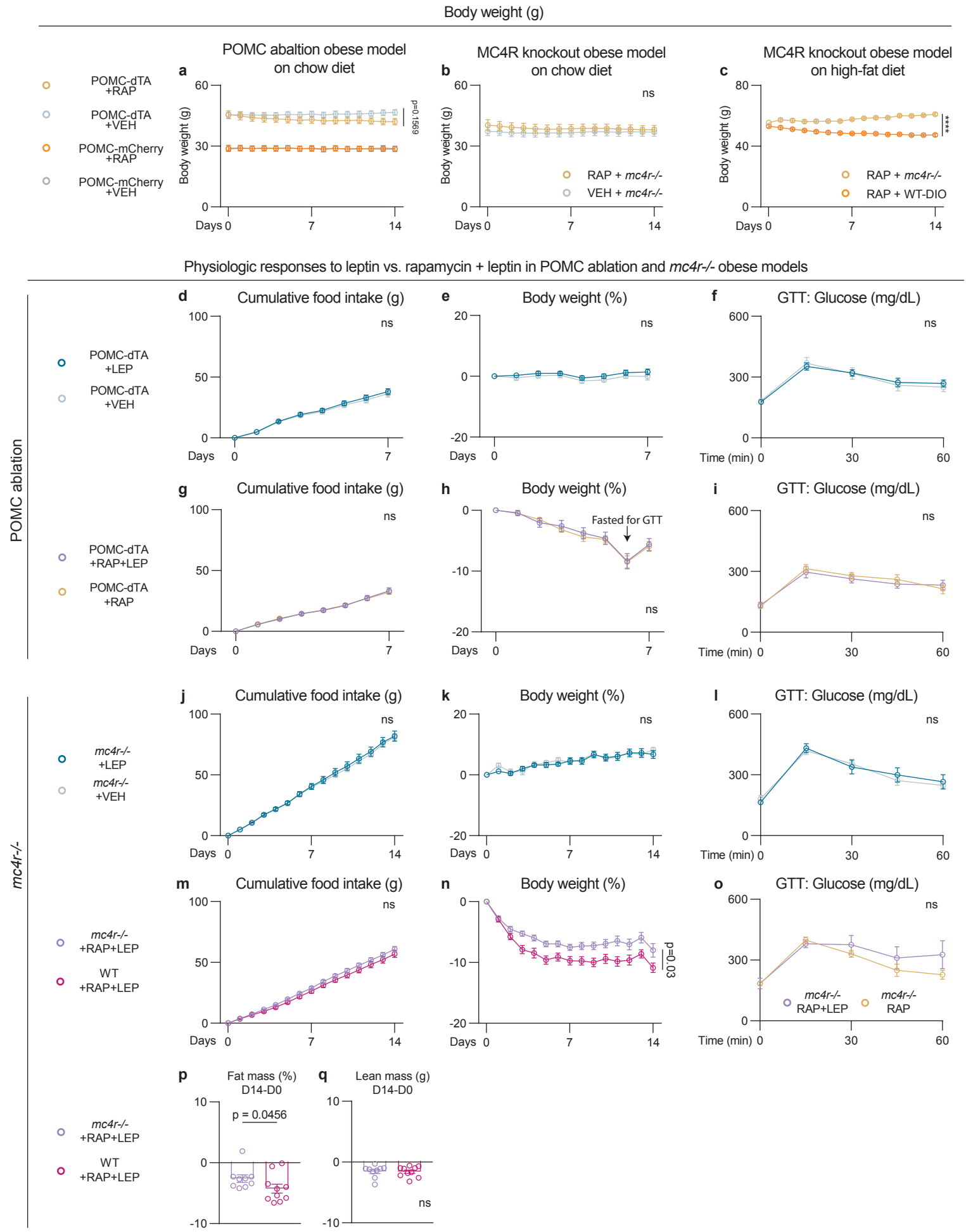
Body weight (g)
POMC abaltion obese model on chow diet
MC4R knockout obese model on chow diet
MC4R knockout obese model on high-fat diet
POMC-dTA +RAP
POMC-dTA +VEH
POMC-mCherry +RAP
POMC-mCherry +VEH
Body weight (g)
Days
p=0.1669
ns
RAP + mc4r-/-
VEH + mc4r-/-
****
RAP + WT-DIO
Physiologic responses to leptin vs. rapamycin + leptin in POMC ablation and mc4r-/- obese models
POMC ablation
mc4r-/-
Cumulative food intake (g)
Body weight (%)
GTT: Glucose (mg/dL)
POMC-dTA +LEP
POMC-dTA +VEH
POMC-dTA +RAP+LEP
POMC-dTA +RAP
Fasted for GTT
Time (min)
mc4r-/- +LEP
mc4r-/- +VEH
mc4r-/- +RAP+LEP
WT +RAP+LEP
p=0.03
mc4r-/- RAP+LEP
mc4r-/- RAP
Fat mass (%) D14-D0
Lean mass (g) D14-D0
p = 0.0456

Figure S7

a

POMC-ablation

8 weeks after AAV delivery in the ARC		14 days treatment	Food Intake	Weight	% Fat	Lean mass
POMC dTA	Obese	RAP	–	↓	–	↓
		VEH	–	–	–	↑
		LEP	–	–	N/A	N/A
		VEH	–	–	N/A	N/A
		RAP+LEP	–	–	N/A	N/A
		VEH	–	–	N/A	N/A
POMC mCherry	Lean	RAP	–	–	–	–
		VEH	–	–	–	–

b

mc4r-/-

Adlibitum on chow for 16 weeks		14 days treatment	Food Intake	Weight	% Fat	Lean mass
mc4r-/-	Obese	RAP	–	↓	–	↓
		VEH	–	↑	↑	–
mc4r-/-	Obese	LEP	–	–	N/A	N/A
		VEH	–	–	N/A	N/A
mc4r-/-	Obese	RAP +LEP	–	↓	↓	–
WT	Lean	RAP +LEP	–	↓↓	↓↓	–

c

Pair-fat on HFD for 16 weeks		14 days treatment	Food Intake	Weight	% Fat	Lean mass	14 days treatment	Food Intake	Weight
mc4r-/-	Obese	RAP	–	↑	↑	–	VEH	–	–
WT-DIO	Obese	RAP	↓	↓	↓	–	VEH	↑	↑

Figure S8

Baseline phsyiologic features of POMC$^{tsc1-/-}$ vs. AgRP$^{tsc1-/-}$ mice models

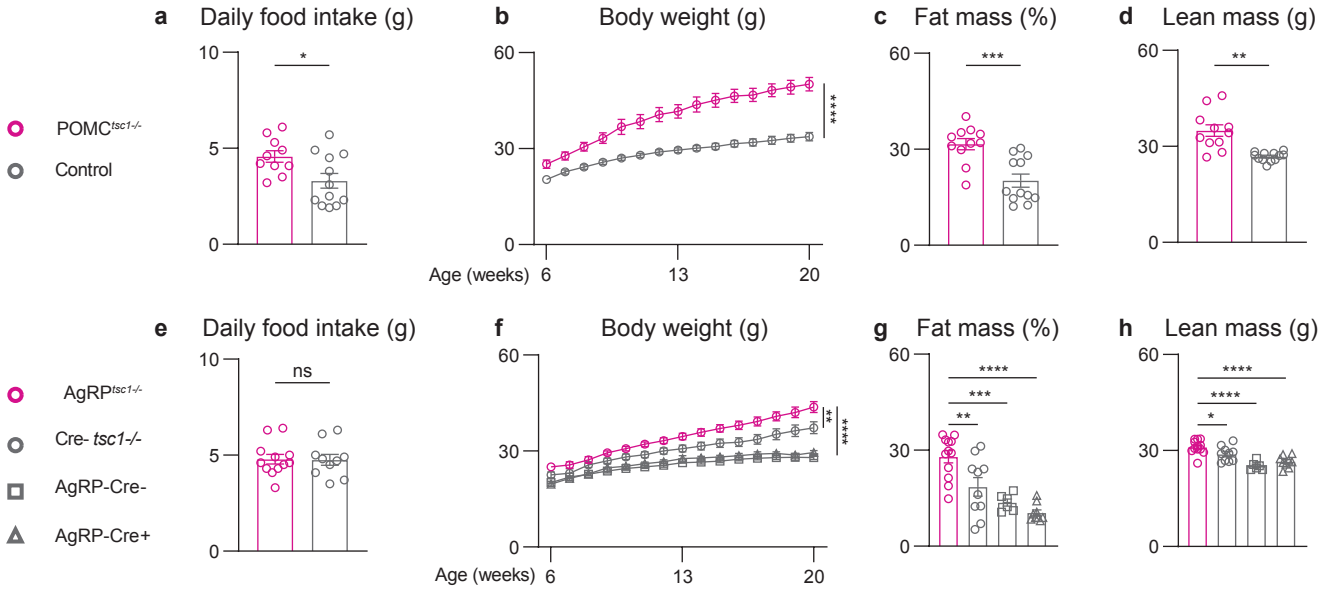

Body weight of ob/ob/POMC$^{tsc1-/-}$ vs. ob/ob/POMC$^{tsc1+/-}$ vs. ob/ob

Figure S9

a

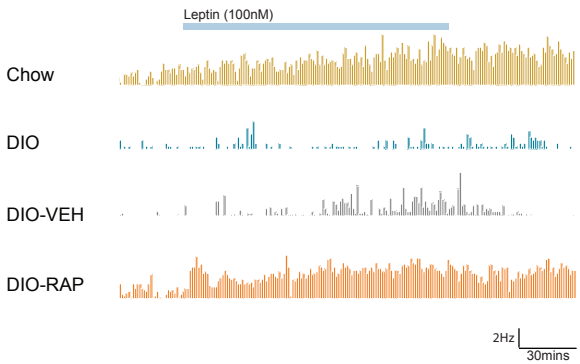

Figure S10

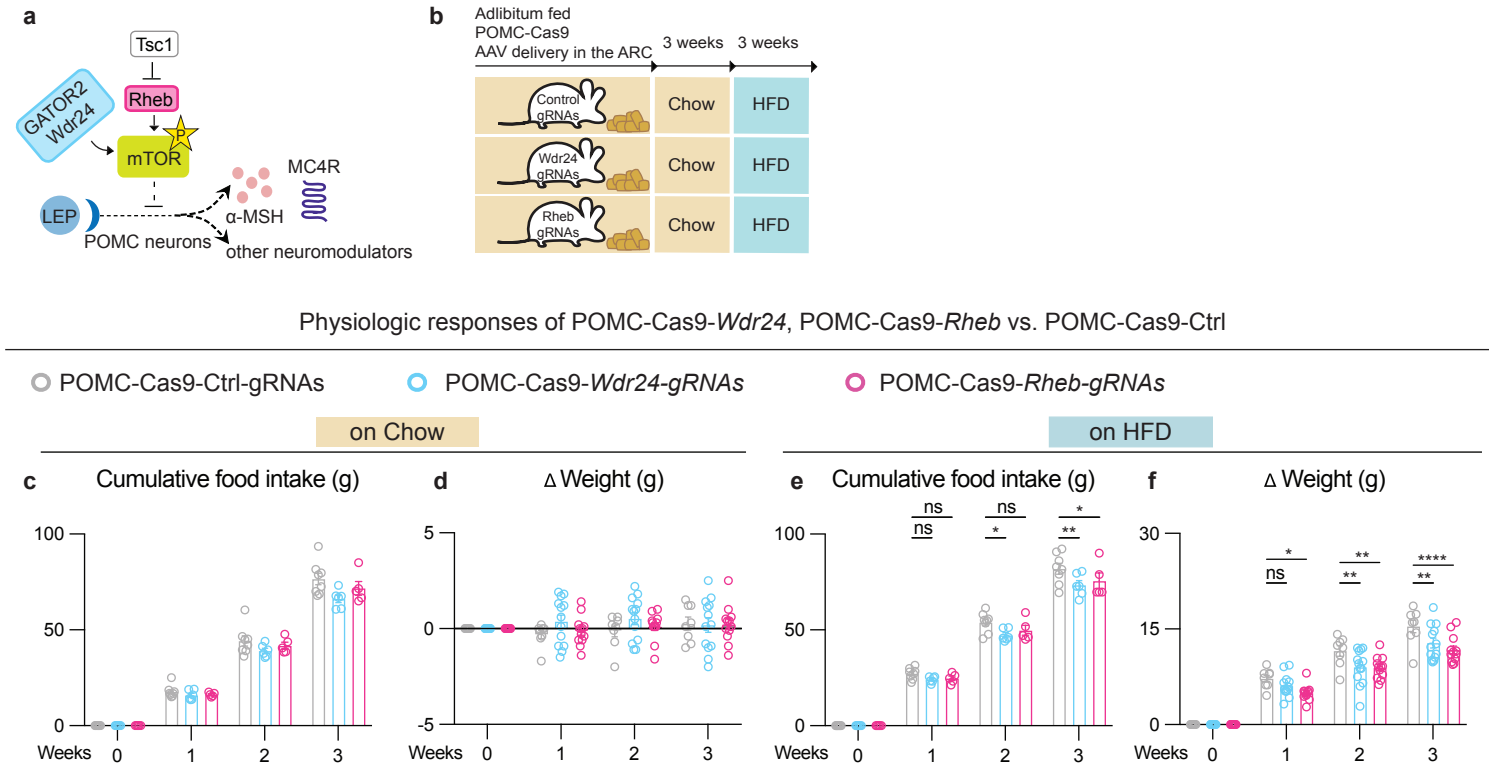
a
Tsc1
Rheb
GATOR2
Wdr24
mTOR
P
MC4R
LEP
α-MSH
POMC neurons
other neuromodulators
b
Adlibitum fed
POMC-Cas9
AAV delivery in the ARC
3 weeks
3 weeks
Control gRNAs
Wdr24 gRNAs
Rheb gRNAs
Chow
HFD
Physiologic responses of POMC-Cas9-*Wdr24*, POMC-Cas9-*Rheb* vs. POMC-Cas9-Ctrl
POMC-Cas9-Ctrl-gRNAs
POMC-Cas9-*Wdr24-gRNAs*
POMC-Cas9-*Rheb-gRNAs*
on Chow
on HFD
c
Cumulative food intake (g)
d
Δ Weight (g)
e
Cumulative food intake (g)
f
Δ Weight (g)
Weeks
ns
*
**
****